THESIS FOR THE DEGREE OF DOCTOR OF PHILOSOPHY

Atom-Diatom Scattering
From Potential Energy Surfaces to Rate Constants

Erik Abrahamsson

UNIVERSITY OF GOTHENBURG

Department of Chemistry
University of Gothenburg
Sweden 2008

Atom-Diatom Scattering -
From Potential Energy Surfaces
to Rate Constants
Erik Abrahamsson
ISBN 978-91-628-7425-4

Cover picture:
An $F(^2P_{1/2})$ atom colliding with
a hydrogen molecule (actual size)

Chalmersbibliotekets reproservice,
Göteborg, Sweden, 2008.

Abstract

This thesis is about the theoretical study of collisions between atoms and diatomic molecules. It might seem like a trivial problem, but in reality it is a highly complex process. Despite, or because of, their apparent simplicity, these processes are of importance for a broad area of science. The applications stretch from the study of fundamental reactions at ultracold temperatures, through the far reaches of space, to the chemistry in the Earth's atmosphere, and combustion at extreme temperatures.

High-level *ab initio* methods (CASSCF/CASPT2) have been used to calculate potential energy surfaces in the linear $^2\Pi$ and $^4\Sigma^-$, and the non-linear $^4A''$ symmetry for the CNO system. The coupling between the collinear $^2\Pi$ and $^4\Sigma^-$ surfaces has been calculated with the CASSCF/RASSI method. The collinear surfaces have been interpolated using a Generalized Discrete Variable Representation method to produce potential energy surfaces as functions of the nuclear coordinates, while the global $^4A''$ surface has been fitted to analytical functions using many-body expansion. Time-dependent wave packet and quasiclassical trajectory calculations are presented for the O + CN reaction on the two collinear surfaces, both with and without coupling between them. Quasiclassical trajectory calculations are presented for the C + NO reaction on the $^4A''$ potential energy surface. The results from the calculations for the C + NO reaction are combined with previously presented results for the $^2A'$ and $^2A''$ surfaces, and compared with experiments. It is seen that the new $^4A''$ surface significantly improves the agreement with experiments. This is the first published study of the $^4A''$ surface for the CNO system.

Time-independent quantum mechanical methods have been used to study the inelastic collision of various atomic and molecular systems, at temperatures ranging from the ultracold to 10 000 K. Rate constants for the fine-structure excitation in the C + H and O + H collisions are presented. These collisions are of interest in astrophysics, as the results can be used to study the chemical evolution in interstellar clouds. The fundamental and very important spin-orbit relaxation of $F(^2P_{1/2})$ and $Cl(^2P_{1/2})$ atoms in a gas of H_2 is investigated, and cross sections and rate constants are presented. Scattering processes at low temperatures in external electric and magnetic fields are also studied. It is shown that the spin-orbit relaxation of polar molecules in a buffer gas of He can be effectively controlled by the field strengths and the angle between the fields, at temperatures easily reached in the lab. This is the first report of the effect of crossed electric and magnetic fields on scattering processes.

Sammanfattning

Denna avhandling behandlar teoretiska studier av kollisioner mellan atomer och diatomära molekyler. Det kan tyckas vara ett trivialt problem, men i själva verket är det en synnerligen komplex process. Trots, eller på grund av, dess enkelhet, är dessa processer av vikt för ett brett område inom vetenskapen. Tillämpningarna sträcker sig från studier av fundamentala kemiska reaktioner vid ultrakalla temperaturer, genom den kalla och nästan tomma rymden, till kemiska processer i jordens atmosfär och förbränning vid extrema temperaturer.

Högkvalitativa ab initio-metoder (CASSCF/CASPT2) har använts för att beräkna potentialenergiytor i de linjära $^2\Pi$ och $^4\Sigma^-$ symmetrierna, och den icke-linjära $^4A''$ symmetrierna för CNO-systemet. Kopplingen mellan de linjära $^2\Pi$ och $^4\Sigma^-$ ytorna har beräknats med CASSCF/RASSI. De linjära ytorna har interpolerats med den generaliserade diskreta variabel representation-metoden, för att ge potentialenergiytor som funktion av avstånden mellan atomerna, medan den globala $^4A''$ ytan har beräknas med en flerkroppsexpansion. Tidsberoende vågpaketberäkningar och kvasiklassiska trajektorieberäkningar presenteras för O + CN reaktionen på de linjära ytorna, med och utan koppling mellan dem. Kvasiklassiska trajektorieberäkningar presenteras för C + NO reaktionen på $^4A''$ potentialenergiytan. Resultaten från C + NO reaktionen kombineras med resultat från de tidigare publicerade $^2A'$ och $^2A''$ ytorna. Det visas att den nya $^4A''$ ytan betydligt förbättrar överensstämmelsen med experimentella studier. Detta är den första publicerade studien av $^4A''$ ytan för CNO systemet.

Tidsoberoende kvantmekaniska beräkningar har används för att studera inelastiska kollisioner mellan ett antal atomer och molekyler, vid temperaturer från ultrakallt till 10 000 K. Hastighetskonstanter för finstrukturexcitation i C + H och O + H kollisioner presenteras. Dessa kollisioner är av intresse inom astrofysiken, då de kan användas för att studera den kemiska utvecklingen i tunna gasmoln i rymden. Den fundamentala och väldigt viktiga spinbanrelaxationen av $F(^2P_{1/2})$ och $Cl(^2P_{1/2})$ i en gas av H_2 studeras, och tvärsnitt och hastighetskonstanter presenteras. Vidare studeras kollisioner mellan polära diatomer och He i elektriska och magnetiska fält vid låga temperaturer. Det visas att spinnbanrelaxationen effektivt kan styras av fältstyrkorna och vinkeln mellan fälten, vid temperaturer som lätt kan uppnås i experiment. Detta är den första studien av effekten av korsade elektriska och magnetiska fält på kollisionsprocesser.

Preface

This thesis is based on, and serves as an introductory text to, the six research papers listed below, henceforth referred to as Paper I – VI. The work has been carried out at the Department of Chemistry, Physical Chemistry, University of Gothenburg, under the supervision of professor Gunnar Nyman, University of Gothenburg, and associate professor Nikola Marković, Chalmers University of Technology, and at the Department of Chemistry, Theoretical Chemistry, University of British Columbia, under the supervision of assistant professor Roman Krems, University of British Columbia.

I. **Classical and quantum dynamics of the O + CN reaction**
Erik Abrahamsson, Stefan Andersson, Nikola Marković, and Gunnar Nyman
Chem. Phys. 324 (2006) 507.

II. **Dynamics of the O + CN reaction on two coupled surfaces**
Erik Abrahamsson, Stefan Andersson, Nikola Marković, and Gunnar Nyman
Manuscript.

III. **Fine-structure excitation of O I and C I by impact with atomic hydrogen**
Erik Abrahamsson, Roman V. Krems, and Alexander Dalgarno
ApJ 654 (2007) 1171.

IV. **Spin-orbit relaxation of F and Cl in a gas of H_2**
Erik Abrahamsson, Gerrit C. Groenenboom, and Roman V. Krems
J. Chem. Phys. 126 (2007) 184303.

V. **Inelastic collisions of cold polar molecules in non-parallel electric and magnetic fields**
Erik Abrahamsson, Timur V. Tscherbul, and Roman V. Krems
J. Chem. Phys. 127 (2007) 044302.

VI. **A new reaction path for the C + NO reaction: Dynamics on the $^4A''$ potential energy surface**
Erik Abrahamsson, Stefan Andersson, Nikola Marković, and Gunnar Nyman
Submitted to PCCP.

Acknowledgements

First of all I would like to thank my supervisor Gunnar Nyman, who always has given me support and never gave up on me, even in the darkest hours. Thank you!

I owe a lot to my co-supervisor Nikola Marković. As was uttered a few years ago, late one night at a dissertation party:
"It's not a pleasure. It's a *!$#@!$@* honor!"

Stefan Andersson, who kick-started me into this project, has given me invaluable help throughout the years. Thank you, Stefan!

Roman Krems, who invited me across the oceans and let me work in his group at University of British Columbia, Vancouver. It was an awesome and very productive year. Cheers, Roman!

To my friends and colleagues, past and present, at the Physical Chemistry group. It has been great working with you! Thank you for making the working days at the chemistry department so much more enjoyable!

Daniel Nilsson deserves a special mention, for all help with Graalen, Ada, Linux, LaTeX, and all the other things I've nagged him about. I'd also like to send an extra thanks to Alpo Karppinen for help with PC related problems.

The people at Theoretical Chemistry at UBC, who made the year in Vancouver what it was. All those long coffee breaks made my day! I will see you soon!

To all my friends, all around the world. What would life be without you?

Mamma och pappa och brorsan, som gjorde det möjligt.

Erik Abrahamsson,
Göteborg, March 2008.

Contents

Chapter 1

Introduction

The study of reaction dynamics is the study of *how* and *why* chemical reactions occur at a molecular level. A chemical reaction is usually, but not always, an effect of two (or more) molecules colliding, sometimes called a scattering process. The collision can result in a chemical reaction, that is, the breaking and forming of bonds and the formation of new molecules. It can also be a non-reactive scattering process, where the molecules collide, transfer energy between each other and move away again, perhaps in new electronic, vibrational or rotational states. Reaction dynamics can be studied experimentally, with high-precision instruments. It is also the focus of theoretical studies, which try to predict or explain experimental results, or find answers that cannot be obtained by experiments. In this thesis I am concerned with theoretical investigations of bimolecular reactions, or rather, a diatomic molecule colliding with an atom. This might seem like a very trivial process, as it only involves three atoms, but as will be seen, it is highly complex.

The present work has two major themes, the first being all about theoretical calculations on a specific chemical system – the reactions between carbon, nitrogen and oxygen atoms. The methods used to study the dynamics of this system are classical trajectories and quantum mechanical wave packet dynamics.

A simplified and intuitive view of classical trajectory dynamics would be thinking of it as launching a marble into a labyrinth, and studying the path it takes. The labyrinth would then represent the potential energy of the system, and each marble the whole chemical system. By releasing a large swarm of marbles - or trajectories - statistical conclusions can be drawn from their final state - their velocities and directions, as well as from their paths through the labyrinth.

Wave packet dynamics is very similar in nature, but due to the Heisenberg uncertainty principle we cannot talk about marbles with known velocity and position. Instead we send a wave, represented by a wave packet that is distributed both in position and velocity, through the labyrinth. We never really know exactly where it is or how fast it is moving, we can only determine its probability distribution. Governed by the Schrödinger equation, the wave packet can travel through walls - or tunnel through barriers, interfere with itself, and be affected by resonances, phenomena not seen in the classical model.

The second part of the thesis is concerned with the study of non-reactive scattering, where the atoms and molecules collide, but do not react. In this work these processes are studied using time-independent quantum dynamics. The idea of using time-independent methods to study the movement and collisions of atoms and molecules, when the system obviously change with time, might at first be counter-intuitive. However, if we consider a constant stream of particles, let them be atoms or molecules, hitting a target, and only look at the incoming stream and the pattern the particles make when they bounce of the target, we see that nothing really changes with time. The same number of particles hit the target every unit of time, and every particle has the same probability of being reflected in a certain direction. Some will bounce back - backward scattering - some will go to the left or right, some will go through the target - forward scattering. Some might even fuse with the target, or tear off pieces of it - a chemical reaction has occurred. By studying the ratio between the scattered wave in a given direction and the incoming wave, we find the so called differential cross-section, a measure of how many of the incoming particles will pass through a given area in space per unit of time after they hit the target. Integration over all angles results in the integral cross-section. The cross-section is tightly coupled with the rate constant, the measure of how many particles undergo a process per unit of time. This is the quantity that tells us how fast a process is.

This thesis continues by giving the outline for how reaction dynamics is studied theoretically, and gives the background to this study by presenting some of the previous work on systems investigated. In Chapter 3 an overview of *ab initio* ("from the beginning", or "first principles") electronic structure calculations, from Hartree-Fock theory to multi-configurational perturbation theory, is given. Different methods to create an electronic potential energy surface from the *ab initio* energy points are presented, and the chapter ends by introducing the spin-orbit coupling.

In Chapter 4 the theoretical foundations for the time-dependent dynamics are laid down. The quasi-classical trajectory (QCT) method is presented, as well as the trajectory surface hopping (TSH) method. The chapter con-

tinues with a discussion on time-dependent wave packet calculations. Attention is given to initiation, propagation, damping, and analysis of the wave packet, as well as propagation on coupled surfaces. An introduction to time-independent quantum dynamics is presented in Chapter 5.

A brief summary of the included papers is given in Chapter 6. Finally, Chapter 7 lets us glance into the future, revealing what might come ahead.

Chapter 2

Background

The general strategy when performing reaction dynamics calculations is to first create the electronic potential energy surface (PES) on which the reaction takes place. The potential energy surface can be created beforehand for the entire multidimensional space - a global potential energy surface, or it can be created locally where needed in each calculation step, as done in direct dynamics. The potential energy surface can also be restricted to a specific symmetry, or specific geometries - known as reduced dimensionality. The surface can be created from experimental data, semi-empirical models or high level *ab initio* calculations. But no matter the choice, dynamics calculations cannot be performed without knowing the potential energy of the system.

After the potential energy surface has been determined, the dynamics of the reaction can be studied. The dynamics can be studied classically or quantum mechanically, time dependently or time independently, on one potential energy surface, or on several coupled surfaces at once. Finally, the reaction has to be analysed, by studying reaction probabilities, reaction times, differential cross-sections, reaction rates, lifetimes of formed complexes, and the energy distribution among the products. The choice of method depends on the properties sought, and on the system to be studied.

2.1 The CNO system

The triatomic system consisting of carbon, nitrogen, and oxygen (known as the CNO or NCO system) has been the focus of many experimental and theoretical studies during the last four decades. The reason for this is mainly the combustion of atomic carbon. By understanding the process of carbon

combustion in a nitrogen and oxygen containing atmosphere, the combustion process can be optimized and the release of unwanted byproducts, like NO_X, minimized. It is no wonder then, that it is the reactions

$$C(^3P) + NO(X^2\Pi) \rightarrow CN(X^2\Sigma^+) + O(^3P) \tag{2.1}$$

and

$$C(^3P) + NO(X^2\Pi) \rightarrow CO(X^1\Sigma^+) + N(^2D) \tag{2.2}$$

that have by far received the most attention of all the possible reactions of the CNO system. There are numerous experimental studies of these reactions, as well as theoretical studies of both the dynamics and kinetics of the reaction (see *e.g.* [1–5] and references therein). The reaction

$$C(^3P) + NO(X^2\Pi) \rightarrow CO(X^1\Sigma^+) + N(^4S) \tag{2.3}$$

has been believed to be of no significance for the formation of CO, and has not been studied in any greater detail. As we show in Paper VI, this assumption is not valid.

The system is also of interest in astrophysics, as for example the CN radical is a known precursor to more complex molecules. Detailed understanding of the CNO system at very low temperatures could give considerable insight into the chemical evolution in dense interstellar clouds [6–11].

Several quasiclassical trajectory calculations (see Refs. [2–5] for work carried out in our group) have been performed for the C + NO reaction, as well as 2D [12] and 3D [13] wave packet dynamics. In the 3D calculations a PES containing the linear CNO minimum but not the deeper NCO minimum was used, which made the 3D study possible for a total angular momentum of zero. In 2001 2D wave packet calculations for the collinear C + NO → CN + O reaction were performed [14].

The reaction between ground state oxygen atoms with cyanogen radicals,

$$O(^3P) + CN(X^2\Sigma^+) \rightarrow CO(X^1\Sigma^+) + N(^2D), \tag{2.4}$$

and

$$O(^3P) + CN(X^2\Sigma^+) \rightarrow CO(X^1\Sigma^+) + N(^4S), \tag{2.5}$$

has not received as much attention as the C + NO reactions. The O + CN reaction is believed to be a major source of depletion of CN in both dense interstellar clouds [6, 7] and combustion [15]. Detailed studies of the reaction were performed in the 1970's by Schmatjko and Wolfrum, including both quasiclassical trajectory (QCT) calculations on empirical LEPS type potential energy surfaces and experimental investigations of the dynamics

and kinetics [16, 17]. From their room temperature experiments they concluded that about 20% of the reactive events produced $CO(X^1\Sigma^+) + N(^4S)$, corresponding to reaction (2.5) above.

Statistical adiabatic channel model (SACM) calculations have been published on the rate coefficients of reaction (2.4) at $T = 300 - 5000$ K [18]. Our group has also performed QCT calculations for the rate coefficients on the same reaction for T between 5 and 5000 K using *ab initio* based potential energy surfaces [5]. In Paper I and II these two reactions are investigated for collinear geometries, using wave packet dynamics.

2.2 Inelastic Non-Reactive Scattering

What happens with two atoms or molecule that collides, but don't react? Do they bounce off in the same state as they came in, or do they transfer energy between each other or within themselves? What determines these processes? Non-reactive processes include quenching of excited states, such as collision-induced relaxation of $N(^2D)$ to $N(^4S)$, or relaxation of fine-structure states, such as $F(^2P_{1/2})$ to $F(^2P_{3/2})$. It can also involve the opposite process, the excitation or activation of atoms and molecules from a lower to a higher state. Non-reactive collisions are also an important cooling process, as in for example buffer gas cooling, where the temperature can be lowered to less than 1 K [19].

In most cases the products of a reaction have a lower potential energy and a greater excess kinetic energy than the reactants. This makes the products less sensitive to small errors in the potential energy surface. The quality of the reactant channel of a reactive system is thus usually of greater importance for a reaction than the product channel. As calculations of non-reactive scattering don't change the colliding species, it is also a good tool to study the accuracy of calculated potential energy surfaces in the reactant channel.

2.2.1 Fine structure excitation of O and C

The fine structure excitations of $O(^3P)$ and $C(^3P)$ by collisions with atomic hydrogen are important cooling processes in planetary atmospheres and in interstellar clouds [20]. Radiative decay of fine structure excited O and C atoms provides diagnostics of the temperature and density of the interstellar clouds [21]. Recent models of interstellar spectra [22, 23] emphasize that the analysis of cooling mechanisms and conditions in the interstellar medium

depends critically on laboratory measurements or calculations of collisional excitation rates. The previous calculations of rates for fine structure excitations in O - H and C - H collisions were reported by Launay and Roueff in 1977 [24], and a refined study of fine-structure excitation rates is needed, as the interaction potentials of the OH and CH molecules have been calculated with much greater precision [25–27]. In Paper III we present rate constants calculated with time-independent methods, using these new potentials.

2.2.2 Fine-structure relaxation of F and Cl

Two important examples of fine-structure relaxations are the relaxations of $F(^2P_{1/2})$ and $Cl(^2P_{1/2})$ in a gas of H_2. The F + H_2 and Cl + H_2 systems have become model examples of chemical physics. The reaction of F with H_2 is a paradigm for exothermic abstraction reactions of atoms with diatomic molecules [28, 29] and the reaction of Cl with H_2 is a prototype of chemical reactions of chlorine with hydrocarbons [29,30], which play an important role in many atmospheric phenomena.

Quantum mechanical calculations have shown that the relative reactivity of the spin-orbit excited $F(^2P_{1/2})$ and $Cl(^2P_{1/2})$ atoms with hydrogen molecules is significantly reduced in comparison with the reaction probabilities of $F(^2P_{3/2})$ and $Cl(^2P_{3/2})$ [28, 31]. This was in agreement with measurements of state-resolved reaction cross sections for fluorine [32] but disagreed with the experiments for chlorine [32–34]. The disagreement has not yet been resolved and it is sometimes attributed to inaccuracies in the theoretical models of Cl - H_2 interactions. The analysis of fine structure relaxation in pre-reactive $F(^2P)$ - H_2 and $Cl(^2P)$ - H_2 complexes may therefore elucidate the mechanisms of the chemical reactions and help resolve the disagreement with the experiment. This is investigated with time-independent dynamics in Paper IV.

2.2.3 Controlling collisions with external fields

With electric fields, molecules may be oriented and aligned in space [35], which allows for measurements of the anisotropy of intermolecular interactions [36–38]. The interaction between molecules and electric fields and lasers have been used in experimental studies of selective bond breaking and bond rearrangement [39], in molecular tomography, which gives 3D "X-ray" images of the molecular orbitals [40, 41], and in the design of a molecular syncrotron [42,43]. Molecules with magnetic dipole moments can be trapped in an inhomogeneous magnetic field if the kinetic energy is less than the po-

tential of the magnetic field forces. In such a magnetic trap the temperatures can be lowered down close to the ultracold regime (<1 mK) [44, 45].

A major drawback of this cooling method is trap-loss, due to collision-induced relaxation to high-field-seeking Zeeman states. It is therefore important to find mechanisms for suppressing spin relaxation in collisions of cold molecules in order to increase the number of trapped molecules in buffer-gas and evaporative cooling experiments (See Refs. [19] and [46] for descriptions of these methods). Recently it has been shown that spin relaxation in $^2\Sigma$ molecules can be manipulated by dc electric fields [47, 48]. A theoretical investigation of the effects of combined electric and magnetic fields at temperatures easily achieved in the lab can show how to manipulate the molecules, and to give understanding of how to minimize the trap loss. A study of the theory and calculations of collisions in combined electric and magnetic fields is found in Paper V.

Chapter 3

Potential Energy Surfaces

As mentioned in Chapter 2, the first thing to do when studying scattering dynamics is to find the potential energy of the system. In this work, we employ *ab initio* methods, based on the Schrödinger equation, to find the potential energy of the system at a large number of geometries. These *ab initio* points are then used to estimate the energy between the points, using well-known mathematical techniques, such as interpolation and analytical fitting. When this is done, the resulting potential energy surface is used to perform the dynamics calculations.

3.1 The Born-Oppenheimer Approximation

The foundation of this work is the non-relativistic Schrödinger equation, presented in 1926. The Schrödinger equation is a wave equation describing the behaviour of matter, and is one of the cornerstones in the theory of quantum mechanics. Solving the Schrödinger equation is a formidable task, and a series of approximations is usually made. When calculating the energies of atoms and molecules, it is generally assumed that the atoms are stationary, and the time-independent Schrödinger equation is used. In 1927 the Born-Oppenheimer approximation was presented. Due to the large mass ratio between the nucleus and the electron (the ratio of the proton to the electron mass is approximately 1836), the movement of the electrons is correspondingly faster than that of the atoms. Born and Oppenheimer made the assumption that the movement of the electron will adjust instantaneously to changes in nuclear configuration. Thus the Schrödinger equation can be separated into an equation defining the nuclear repulsion and an electronic Schrödinger equation describing the electron-electron and the

electron-nuclear interactions. The Born-Oppenheimer approximation is fundamental to both electronic structure theory and to molecular dynamics, second in importance only to the Schrödinger equation itself, as it allows for the construction of potential energy surfaces.

The electronic Schrödinger equation can be written as

$$\hat{H}_{\text{el}}\Psi_{\text{el}} = E_{\text{el}}\Psi_{\text{el}} \tag{3.1}$$

where

$$\hat{H}_{\text{el}} = -\frac{1}{2}\sum_i \nabla_i^2 - \sum_{i,A}\frac{Z_A}{r_{iA}} + \sum_{i>j}\frac{1}{r_{ij}} \tag{3.2}$$

is the electronic Hamiltonian, expressed in atomic units. Here r_{iA} is the distance between electron i and nucleus A, r_{ij} is the distance between electron i and j, Ψ_{el} is the electronic wave function, and E_{el} is the electronic energy for a given nuclear geometry. The total energy, or the potential energy, of the system is thus the sum of the electronic energy E_{el} and the nuclear-nuclear repulsion:

$$V(\mathbf{R}) = E_{\text{el}}(\mathbf{R}) + \sum_{A,B}\frac{Z_A Z_B}{R_{AB}}, \tag{3.3}$$

where $\mathbf{R}$ is the nuclear positions and R_{AB} is the distance between nuclei A and B. This chapter is dedicated to solving the electronic Schrödinger equation, Eq. 3.1, and finding the electronic potential energy $V(\mathbf{R})$.

3.2 The Hartree-Fock Method

The Hartree-Fock method has, at least before the quite recent acceptance of density functional theory (DFT), been *the* method of choice when performing quantum chemistry. In Hartree-Fock theory, the electron-electron interaction is approximated by assuming that each electron moves in an average electric field created by all other electrons. In this way the explicit electron-electron interaction is neglected, and Eq. 3.1 is reduced to a series of coupled differential equations, each only involving one electron. This allows the construction of Fock operators, which act as effective Hamiltonians for the electrons.

The Fock operators depend on all orbitals, forcing the solution to be known before the Hartree-Fock equations can be solved. Thus, the Hartree-Fock equations have to be solved by an iterative procedure, known as the self-consistent field (SCF) procedure. An initial guess is made as to the nature of the molecular orbital, the 'field', and the Hartree-Fock equations are solved until the resulting orbitals do not change (significantly) between iterations, i.e. the Fock operator is consistent with itself.

The Hartree-Fock method has the advantage of being relatively fast compared to many other methods, and generally producing results that at least give trends that follow experimental or exact results. The main drawback of the Hartree-Fock method is the inability to account for correlation energy. The correlation energy is usually separated into two parts: a *dynamic* correlation, which is the effect of the cross-terms r_{ij}^{-1} in Eq. 3.2, and a *static* correlation. The observation of static correlation is an effect of the single determinant used in Hartree-Fock theory to describe the wave function. The correlation occurs when several separate electronic configurations are of near equal importance for describing the system, which cannot be accounted for by Hartree-Fock theory.

The correlation energy is usually defined as the difference between the Hartree-Fock limit (the Hartree-Fock energy obtained with the largest effective basis set) and the true energy [49]. The correlation energy is generally not large, compared to the total energy, but to characterize properties such as chemical bonds, the difference between two energies is sought. Since this means taking the difference between two large numbers, the correlation may be of great importance. Correlation energy is also of great importance when studying open-shell systems - such as the NCO system.

Although the Hartree-Fock method has many drawbacks, it is still very important in nearly all *ab initio* calculations. Since it is reasonably accurate, and computationally cheap, the resulting wave functions serve as an excellent starting point for more accurate methods.

3.3 Perturbation Theory

Often it is possible to write the Hamiltonian of a problem that cannot easily be solved in two parts, one unperturbed (zeroth order) part that can easily be solved, and one part that represents a perturbation of the original problem. The most commonly used perturbation theory is the Møller-Plesset Perturbation Theory (MPPT), suggested by Rayleigh and Schrödinger, and applied in 1934 by the Danish scientists Møller and Plesset [50]. Second order Møller-Plesset perturbation theory (MP2) results in significant improvements over Hartree-Fock theory, and is relatively computationally cheap (first order MPPT - MP1 - results in the Hartree-Fock energy). Higher-order corrections can be made (MP3, MP4, etc) to improve the results by recovering more of the correlation energy. MP3 has no major advantage over MP2, and in practice only MP2 or MP4 are used [51].

The main advantages of MPPT are that it is both size-consistent and size-extensive, if the reference function is so [49]. This means that MPPT

can be used to correctly represent chemical reactions. However, MPPT is not variational, and the energy calculated no longer has a lower bound in the exact value. This problem is generally quite small, and MPPT theory has gained widespread use.

3.4 Multi-Configurational Methods

Whereas MPPT methods can recover most of the dynamic correlation, it still cannot account for the static correlation that occurs when more than one electron configuration is of importance for describing the system. The MPPT methods still rely on one determinant to describe the system, which is generally enough for most closed-shell systems. But for open-shell systems, such as for example the NCO system studied here, the static correlation is large, and single configuration methods are inadequate.

By exchanging the single configurational HF wave function with a sum over all probable configurations, the static correlation is accounted for. Within this sum, each configuration is given a weight (configuration interaction coefficient), which is optimized together with the orbitals. This is known as the multi-configurational self-consistent field (MCSCF) method. In practice, the length of the MCSCF expansion is finite and quite limited, due to numerical constraints connected with the simultaneous optimization of the orbitals and CI coefficients. While the static correlation is at least partly determined by this method, choosing the proper set of configurations is problematic. To standardize the selection of configurations, the complete active space SCF (CASSCF) method [52] has been developed. In this method, the orbital space is divided into three subspaces: the *inactive*, *active*, and *secondary* orbital spaces. The inactive orbitals are orbitals that are always doubly occupied, typically the core orbitals, while the active orbitals are the valence orbitals, with no restrictions on the occupation number. Finally, the secondary orbitals are virtual orbitals that are always left unoccupied. CASSCF is not inherently size-consistent, but the active space can be chosen such that size-consistency is achieved. The upper limit for performing CASSCF calculations is for about 12-15 active orbitals, making the NCO system one of the largest systems that can be treated with all valence electrons in the active orbital space.

CASSCF is a zeroth order method, and even though the static correlation is recovered, the dynamic correlation, caused by the electron-electron repulsion, is not included. The CASPT2 (complete active space second-order Perturbation Theory) method is a multi-configurational reference function second-order perturbation method (see for example Ref. [49]). The

CASSCF wave function, which contains the static correlation, is used as multi-configurational reference function for the MP2 method, which includes the dynamic correlation. CASPT2 is generally a very effective method for calculating a global potential energy surface.

A CASPT2 calculation is made in three steps: First a Hartree-Fock calculation is performed to give a starting wave function for the subsequent CASSCF calculation, in which the static correlation is retrieved. The CASSCF wave function is then used as reference function for the CASPT2 calculation, which is the third and final step.

3.5 Creating a Potential Energy Surface

Even today, despite the rapid improvement in both computer architecture and computational algorithms, *ab initio* calculations are very computationally time-consuming, and dynamic calculations may demand hundreds of thousands, or even millions, of energy evaluations to be accurate. Thus, methods have been developed to accurately evaluate the potential energy between the *ab initio* energy points, allowing the creation of an arbitrary number of energy points from a limited set of *ab initio* calculations.

Usually about 10^N, where N is the number of independent coordinates, energy points are needed for an accurate description of the full potential energy surface. The energies at short ranges are preferably calculated by some *ab initio* method, like the ones described above. Calculations of the long-range interactions are usually simplified by approximating the wave function of the whole system (in our case a triatomic system) as the product of the wave function of the fragments (which in our case is a diatomic fragment and an atom). The electronic energies of the fragments are calculated separately, and the remaining interaction energy is calculated as the sum of electrostatic, induction and dispersion interaction energies. How this can be applied in the interaction between an atom and diatomic molecule is described in detail in Ref. [3].

To calculate the electronic potential energy in between the calculated energy points, various methods can be used. The oldest method has been to fit the energy points to a set of analytical functions. Common function types are LEPS (London-Eyring-Polanyi-Sato) [53] functions and MBE (many-body expansion) [54]. When fitting an analytical function to the energy points, the energy at the points is not reproduced exactly, but is optimized by means of a least square fit. Analytical fitting usually involves many unknown parameters, and the accuracy of the resulting surface depends on the choice of functional form, and requires skill and insight to produce an accurate

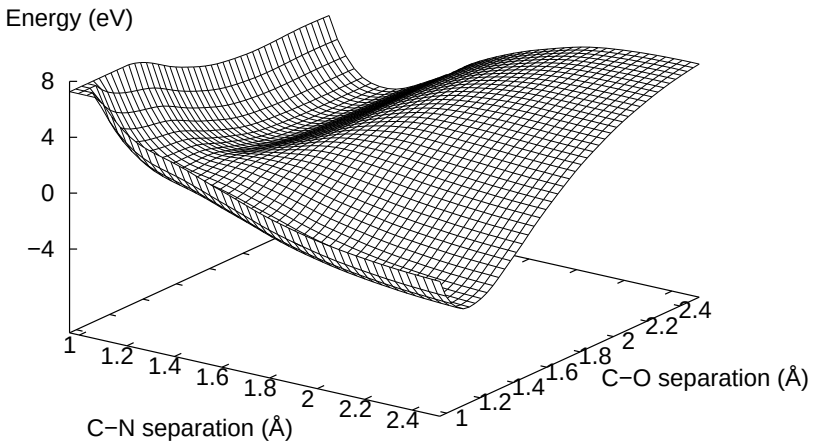

Figure 3.1: The collinear $^4\Sigma^-$ surface for the O+CN reaction, representing a typical potential energy surface. The surface is interpolated by GDVR from 484 energy points, of which 171 are CASPT2 *ab initio* energy points.

potential energy surface.

In the last ten to fifteen years, different interpolation procedures for constructing potential energy surfaces have gained increased popularity. Interpolation methods reproduce the input energy points exactly, as opposed to the fitting procedures. However, it does not guarantee proper behaviour between the grid points, where unphysical oscillations may occur. The review by Nyman and Yu [55] contains a brief summary, including references, of the most commonly used methods.

In the present work the generalized discrete variable representation (GDVR) method [56], developed in our group, has been used in the study of the collinear O+CN system. It has previously been successfully applied to reduced dimensionality descriptions of the OH+HCl [57] and CH_3+HBr [58] reactions and to create a 3D potential energy surface for the HCBr molecule [59]. We have also applied a many body expansion with analytical functions developed by Aguado and Paniagua [60] to fit three dimensional *ab initio* data of the CNO system in $^4A''$. This method has previously been applied to the $^2A''$ and $^2A'$ surfaces of the CNO system [3–5].

3.6 Spin-Orbit Interaction

So far we have only been concerned with non-relativistic quantum mechanics. Spin-orbit coupling, however, requires a relativistic treatment of the atom. This is far beyond the scope of this text, and fortunately spin-orbit coupling can at least be understood by a much simpler semi-classical treatment.

From classical mechanics we know that a magnetic dipole moving in an electrostatic field will experience a force proportional to its velocity and the strength of the field. If we consider an electron moving in a central field, for example the effective potential energy of an unpaired electron moving around an atom, there will be a coupling between the spin magnetic moment of the electron, and its magnetic moment due to the orbital movement. This effect is called spin-orbit coupling, and will shift the energy up or down, depending on the sign of the spin of the electron.

This rather naive model of spin-orbit coupling can still give qualitative insight in the properties of the spin-orbit interaction. With the help of classic electromagnetic theory, it can be shown that the spin-orbit coupling contribution to the total energy is proportional to $\boldsymbol{L}\cdot\boldsymbol{S}$, where $\boldsymbol{L}$ and $\boldsymbol{S}$ are the electronic orbital and spin angular momenta, which is the same relation given by the full relativistic treatment (see for example [61]). The presence of spin-orbit interaction leads to a break-down of the Born-Oppenheimer approximation. The electronic states become coupled, whereby the system may jump between states, jumps that normally, in the absence of spin-orbit interaction, are spin-forbidden.

Chapter 4

Time Propagation

Once the potential energy surface for the system is found, we can begin our study of the dynamics of the system. In the following section time-dependent dynamics will be discussed, starting with classical dynamics, based on the work of Sir Isaac Newton in the late 17^{th} century.

4.1 Classical Dynamics

Classical trajectory calculations are the computationally cheapest method for studying reaction dynamics. In many cases trajectory calculation is the only available option, as quantum dynamics is generally not feasible except for small and light systems. A trajectory is defined as the set of position and momentum coordinates of a moving point in phase space as a function of time. By following this trajectory, the time evolution of the reaction can be studied (Fig. 4.1). It is important to note that the trajectory defines the whole system and its properties.

In classical trajectory dynamics, Newton's equations of motion,

$$-\frac{\partial V}{\partial q_i} = m_i \frac{d^2 q_i}{dt^2} \tag{4.1}$$

are solved for a set of initial conditions of the system. The solution to Eq. 4.1 is the path that the system will follow on the potential energy surface V. The main aspects of classical trajectory calculations are finding the potential energy surface of the system as described in the previous chapter, sampling the initial conditions, choosing an appropriate integrator for solving Newton's equations of motion, and analysing the trajectories [62].

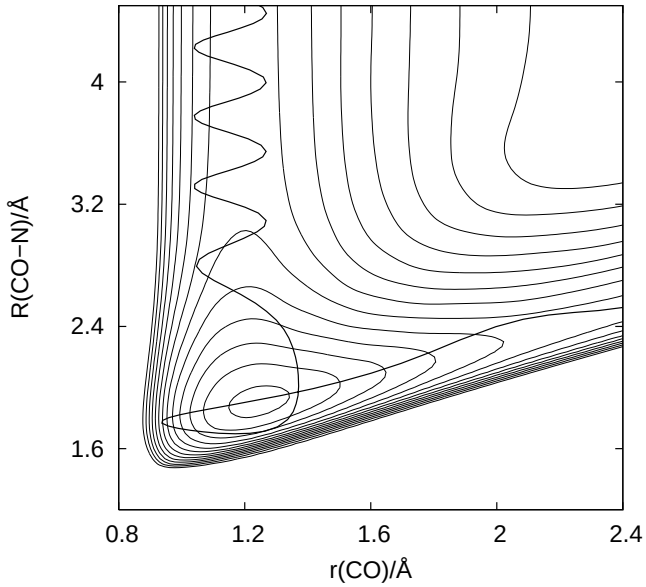

Figure 4.1: A quasiclassical trajectory. The trajectory illustrates the process $O + CN(v = 0) \rightarrow N + CO(v' = 2)$ on the collinear $^2\Pi$ potential energy surface.

4.1.1 Quasiclassical Trajectories

The difference between classical and quasiclassical trajectory calculations (QCT), is the inclusion of zero point energy, which is a pure quantum effect, in the initial conditions of QCT. For small systems, this inclusion of the zero point energy generally gives better agreement with quantum calculations than pure classical trajectory calculations. Except for large systems, QCT is the standard method for investigating reaction dynamics classically [63].

4.1.2 Trajectory Surface Hopping

When two potential energy surfaces are coupled, through for example spin-orbit coupling, trajectory surface hopping (TSH) calculations can be used to allow the trajectory to jump between the surfaces. The methodology used here is based on the formulation given by Stine and Muckerman [64–66], where the dynamics is carried out on the adiabatic surfaces. When the two surfaces are sufficiently close, Landau-Zener theory [64] is used to determine if the system will undergo a non-adiabatic transition, *i.e.*, jump between the two adiabatic surfaces.

4.2 Wave Packet Dynamics

In wave packet dynamics a wave packet representing the state of the system is propagated on a potential energy surface by solving the time-dependent Schrödinger equation,

$$i\hbar\frac{\partial}{\partial t}\Psi(\mathbf{R},t) = \hat{H}\Psi(\mathbf{R},t) \tag{4.2}$$

where the Hamiltonian operator is given by

$$\hat{H} = \hat{T} + \hat{V} = -\frac{\hbar^2}{2\mu}\nabla^2 + V(\mathbf{R}). \tag{4.3}$$

In Eq. 4.3, the potential $V(\mathbf{R})$ is obtained by solving Eq. 3.3 for each nuclear position $\mathbf{R}$. The formal solution to Eq. 4.2 is

$$\Psi(t) = \hat{U}(t,t_0)\Psi(t_0) \tag{4.4}$$

where $\hat{U}$ is the time-evolution operator, given by

$$\hat{U}(t,t_0) = \mathrm{e}^{-i\hat{H}(t-t_0)/\hbar}, \tag{4.5}$$

provided that the Hamiltonian is explicitly time-independent. The Hamiltonian $\hat{H}$ is an operator, making the time-evolution operator $\hat{U}$ an exponential function of an operator, which cannot be applied directly, since the potential and kinetic energy operators in the Hamiltonian do not commute ($\hat{T}\hat{V} \neq \hat{V}\hat{T}$).

4.2.1 The Initial Wave Packet

If we, as in Paper I and II, consider the case of the O + CN system for collinear geometries, the time-dependent wave packet calculations can be carried out in mass-weighted product Jacobi coordinates $(\tilde{R},\tilde{r})$. The Hamiltonian can then be written as

$$\hat{H} = -\frac{\hbar^2}{2\mu}\left(\frac{\partial^2}{\partial\tilde{R}^2} + \frac{\partial^2}{\partial\tilde{r}^2}\right) + V(\tilde{R},\tilde{r}), \tag{4.6}$$

where $\tilde{R}$ is the mass-weighted center-of-mass separation between N and CO, $\tilde{r}$ is the mass-weighted CO bond distance, and the reduced mass μ is given by

$$\mu = \left(\frac{m_\mathrm{O}m_\mathrm{C}m_\mathrm{N}}{m_\mathrm{O}+m_\mathrm{C}+m_\mathrm{N}}\right)^{1/2}. \tag{4.7}$$

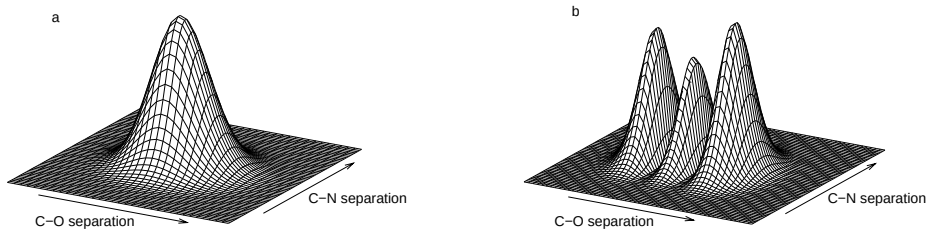

Figure 4.2: Asymptotic wave packets according to Eq. 4.10 for $CO(X^1\Sigma^+)$ + $N(^4S)$ with CO in the vibrational ground state (a) and second exited state (b).

The product Jacobi coordinates are given by

$$R = \alpha^{-1}\tilde{R}, \tag{4.8}$$
$$r = \alpha\tilde{r}, \tag{4.9}$$

where $\alpha = (\mu_R/\mu_r)^{1/4}$ and μ_R and μ_r are the reduced masses corresponding to the N-CO and CO systems, respectively. The initial wave packet is set up in reactant Jacobi coordinates, as a product of a vibrational eigenfunction of the CN system, $\phi(r_{\mathrm{CN}})$, and a translational function in the form of a Gaussian wave packet, $\chi(R_{\mathrm{O-CN}})$,

$$\Psi(R_{\mathrm{O-CN}}, r_{\mathrm{CN}}, t = 0) = \phi_v(r_{\mathrm{CN}})\chi(R_{\mathrm{O-CN}}). \tag{4.10}$$

The wave function is then transformed to product Jacobi coordinates before the propagation begins. The vibrational eigenfunctions needed for the initialization and analysis are obtained by solving the time-independent Schrödinger equation for the diatomic fragments using a sine-basis expansion of the wave function. Fig. 4.2 shows examples of two initial wave packets for $CO(X^1\Sigma^+)$ + $N(^4S)$.

4.2.2 Split Operator Method with Fast Fourier Transforms

There are several numerical methods for solving the time-dependent Schrödinger equation. A detailed discussion of these can be found in e.g. ref. [67]. The method used throughout our studies is the (second order) split-operator method, combined with fast Fourier transforms [68]. In this method the time-evolution operator is approximated by a splitting of the

Hamiltonian. The Hamiltonian can be split such that the kinetic energy operator is between potential energy operators, referred to as the *kinetic referenced* split operator method,

$$e^{-i(\hat{T}+\hat{V})\Delta t/\hbar} = e^{-i\hat{V}\Delta t/2\hbar} e^{-i\hat{T}\Delta t/\hbar} e^{-i\hat{V}\Delta t/2\hbar} + O(\Delta t^3). \tag{4.11}$$

The validity of Eq.4.11 can be proved by Taylor expanding the left and right sides. The approximated time-evolution operator, Eq. 4.11, is Hermitian. It also conserves the norm of the propagated wave packet, which is an important property of the wave packet.

Choosing between kinetic referenced split operator method, shown in Eq 4.11, or the *potential referenced* split operator method, where the potential energy operator is between kinetic energy operators,

$$e^{-i(\hat{T}+\hat{V})\Delta t/\hbar} = e^{-i\hat{T}\Delta t/2\hbar} e^{-i\hat{V}\Delta t/\hbar} e^{-i\hat{T}\Delta t/2\hbar} + O(\Delta t^3), \tag{4.12}$$

is a matter of choice. Throughout this study, we have employed the kinetic referenced split operator method.

To solve the Schrödinger equation, the Hamiltonian has to operate on the wave packet at each time step. The potential part of the Hamiltonian is trivial, as it is local, *i.e.* the wave packet Ψ only has to be multiplied by the exponent of the potential energy V at each grid point. The kinetic part of the Hamiltonian involves a Laplacian operator (∇^2), which is a non-local operator in coordinate space. By transforming the wave packet to momentum space, via a Fourier transform, the Laplacian can be evaluated as a local operator. The Fourier transform $\hat{F}$ is defined as

$$\hat{F}(\Psi) = \phi(k) = \frac{1}{\sqrt{2\pi}} \int_{-\infty}^{\infty} \mathrm{d}x \Psi(x) e^{-ikx} \tag{4.13}$$

and the inverse Fourier transform $\hat{F}^{-1}$ as

$$\hat{F}^{-1}(\phi) = \Psi(x) = \frac{1}{\sqrt{2\pi}} \int_{-\infty}^{\infty} \mathrm{d}k \phi(k) e^{ikx}. \tag{4.14}$$

It can easily be shown that the second order derivative of the wave function can be written as

$$\frac{d^2\Psi(x)}{dx^2} = \frac{1}{\sqrt{2\pi}} \int_{-\infty}^{\infty} \mathrm{d}k \phi(k) (ik)^2 e^{ikx}. \tag{4.15}$$

It is seen that the second order derivative is a simple multiplication by $(ik)^2$ in momentum space.

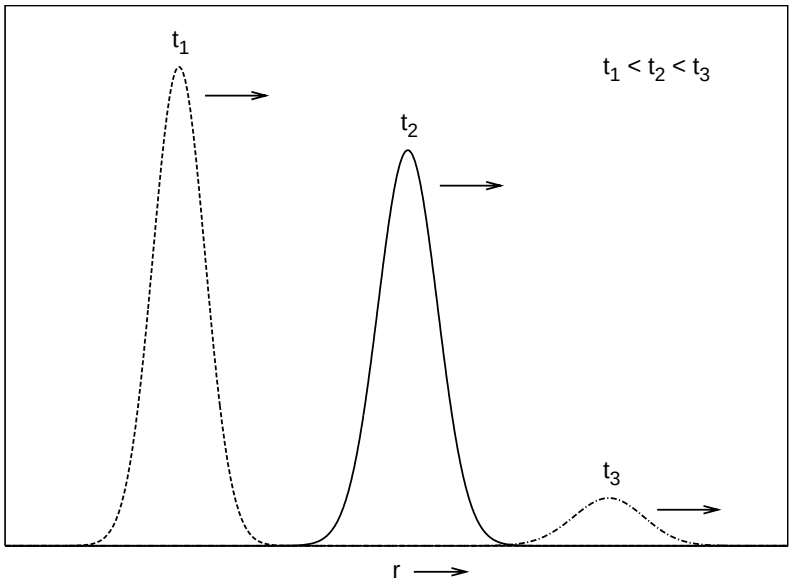

Figure 4.3: A wave packet is damped as it propagates through the damping region.

The algorithm for propagating the wave packet using the kinetic referenced split operator method is as follows: First the wave function is multiplied by $e^{-i\hat{V}\Delta t/2\hbar}$. This new function is Fourier transformed to momentum space and multiplied by the free particle operator $e^{-i\Delta t k^2\hbar/2\mu}$. An inverse Fourier transform is applied, and finally the function is again multiplied by $e^{-i\hat{V}\Delta t/2\hbar}$, which completes the time step. Thus, each time step involves one Fourier transform, one inverse Fourier transform and three simple multiplications. Using the fast Fourier transform, the calculation time scales with the grid-size in the order of $N \log N$.

4.2.3 Damping Function

The discrete Fourier transform requires the function to be periodic. Therefore, in our case, the wave packet has to be damped, if the wave packet is not to pass through the boundaries of the grid and reappear at the other end, or be non-physically reflected from the boundary. These effects are avoided by damping the wave function (Fig. 4.3) between a point r_d and the boundary of the grid, r_max, in each coordinate:

$$f(r_i) = \begin{cases} 1, & r_i < r_\mathrm{d}, \\ \exp\left[-V_\mathrm{d}\Delta t/\hbar\right], & r_i \geq r_\mathrm{d} \end{cases}, \tag{4.16}$$

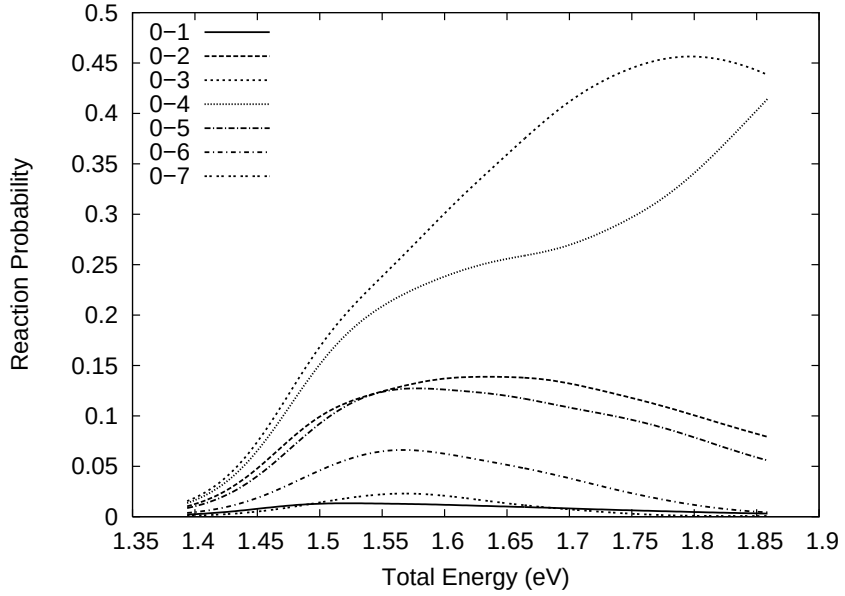

Figure 4.4: The state to state ($v - v'$) reaction probability for the collinear $O(^3P) + CN(X^2\Sigma^+) \rightarrow CO(X^1\Sigma^+) + N(^4S)$ reaction. The wave packet is initiated in the vibrational ground state, $v = 0$. The same data is presented in a different manner in Paper I, Fig. 7.

where V_d is the exponential damping function suggested by Vibók and Balint-Kurti [69]. We have also introduced a time-dependent scale factor in the exponential damping function V_d, to account for the variation of the average product kinetic energy with time.

4.2.4 Analysis of the Scattered Wave Packet

The time propagation of the wave packet does not give much information in itself. The really interesting information is the state-to-state reaction probabilities. We start the wave packet in a given vibrational state (Eq. 4.10), so we get the probabilities for going from *one given* vibrational state in the reactant arrangement to *all* vibrational states in the product arrangement. These probabilities are found by, at a point R_p, before applying the damping function, projecting the scattered wave packet onto asymptotic vibrational eigenstates $\phi_{v'}(r)$:

$$c_{v'}(t) = \int \mathrm{d}r \phi_{v'}(r) \Psi(R_p, r, t). \tag{4.17}$$

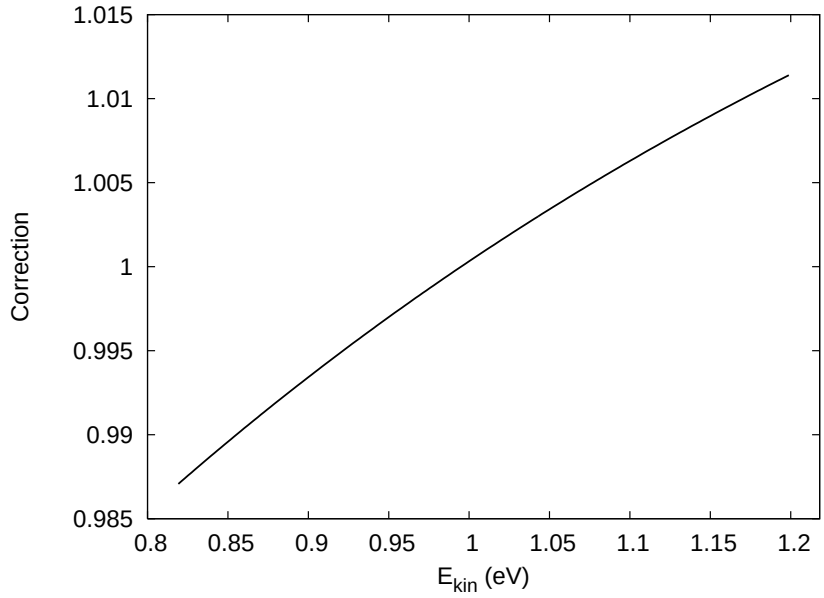

Figure 4.5: Example of a correction function. $\bar{E}_{\mathrm{kin}} = 1.0$ eV in the $\mathrm{O}(^3\mathrm{P}) + \mathrm{CN}(\mathrm{X}^2\Sigma^+)$ channel on the $^2\Pi$ surface.

The time-dependent amplitudes $c_{v'}$ are Fourier transformed to energy space

$$b_{v'} = \frac{1}{\sqrt{2\pi}} \int \mathrm{d}t c_{v'}(t) \exp\left(iEt/\hbar\right), \tag{4.18}$$

and the state-to-state reaction probabilities (Fig. 4.4) are computed from the ratio between the scattered and incident fluxes [70],

$$P_{v \to v'}(E) = \frac{F_{v'}(E)}{F_v(E)}, \tag{4.19}$$

where

$$F_{v'}(E) = \frac{1}{\mu_{\mathrm{OC-N}}} k_{v'} \mid b_{v'}(E)\mid^2, \tag{4.20}$$

$$k_{v'} = \frac{1}{\hbar}\sqrt{2\mu_{\mathrm{OC-N}}(E - V(R_{\mathrm{p}}) - E_{v'})}\,. \tag{4.21}$$

To avoid dividing by values near zero in Eq. 4.19, the outgoing wave packet is analysed in an energy interval corresponding to 95% of the energy distribution in the incident Gaussian.

The incident flux, $F_v(E)$, is, in principle, given by an analytical expression [70], but since the potential has not reached its true asymptotic value at

the position of the initial wave packet, a small correction is needed. The correction to the Gaussian distribution, illustrated in Fig. 4.5, is simply to obtain the probability distribution of the incident k-values by propagating the initial Gaussian wave packet $\chi(R)$ backwards. This k-distribution is then used to normalize the scattered components, rather than the initial Gaussian distribution.

4.2.5 Dynamics with Coupled Surfaces

In cases with two coupled potential energy surfaces, as in Paper II, the Hamiltonian in (Eq. 4.6) must be changed, due to the fact that the potential energy operator now is a matrix:

$$\hat{V} = \begin{pmatrix} V_1 & V_{12} \\ V_{12}^* & V_2 \end{pmatrix}, \tag{4.22}$$

where V_1 and V_2 are the diabatic potential energy terms, and V_{12} are potential coupling terms. The Schrödinger equation now becomes

$$i\hbar\frac{\partial}{\partial t}\begin{pmatrix} \Psi_1 \\ \Psi_2 \end{pmatrix} = \left[\begin{pmatrix} \hat{T} & 0 \\ 0 & \hat{T} \end{pmatrix} + \begin{pmatrix} V_1 & V_{12} \\ V_{12}^* & V_2 \end{pmatrix}\right]\begin{pmatrix} \Psi_1 \\ \Psi_2 \end{pmatrix}. \tag{4.23}$$

In order to solve Eq. (4.23), the potential energy matrix has to be diagonalized at each grid point by the unitary transformation

$$\boldsymbol{D} = \boldsymbol{U}^\dagger \boldsymbol{V} \boldsymbol{U}, \tag{4.24}$$

where $\boldsymbol{D}$ is diagonal. The diagonal elements of the matrix $\boldsymbol{D}$ form two non-crossing, adiabatic surfaces. The exponential function of the matrix $\boldsymbol{V}$ can now be written as

$$\mathrm{e}^{\boldsymbol{V}} = \boldsymbol{U}\mathrm{e}^{\boldsymbol{D}}\boldsymbol{U}^\dagger, \tag{4.25}$$

and the split-operator method can be used to propagate the wave packet on the two coupled electronic surfaces.

Chapter 5

Time-Independent Dynamics

Previously we have been solving the time-dependent Schrödinger equation (Eq. 4.2) for a molecular system. However, if there are no external fields, such as light, or oscillating electric or magnetic fields, that explicitly depend on time, we can separate the time-dependence from the equation. The solution for the time-evolution is a trivial exponential function, given in atomic units by

$$\hat{U} = \exp(-\mathrm{i}Et), \tag{5.1}$$

which only changes the phase of the wave function, but not its magnitude. In the following sections we will discuss how we can solve the remaining problem, the time-independent scattering, for some inelastic collisions between atoms and molecules.

5.1 The Inelastic Scattering Problem

Consider the simple case of two atoms colliding and scattering off each other, without reacting. If the collision is inelastic, the atoms can undergo fine structure or electronic transitions, and scatter with different translational energies. Let for example one of the atoms be an oxygen atom, and the other a hydrogen atom, both atoms in their ground states,

$$\mathrm{O}(^3\mathrm{P}_2) + \mathrm{H}(^2\mathrm{S}_{1/2}) \rightarrow \mathrm{O}(^3\mathrm{P}_{j_\mathrm{O}}) + \mathrm{H}(^2\mathrm{S}_{1/2}). \tag{5.2}$$

We can solve the Schrödinger equation, Eq. 4.2, for this system using wave packets, as described in Section 4.2 above. But when the Hamiltonian $\hat{H}$ does not explicitly depend on time, the time-dependence of the wave function Ψ

may be separated and the Schrödinger equation is reduced to

$$\hat{H}\psi = E\psi, \tag{5.3}$$

where E is the total energy of the system, and ψ is the time-independent part of Ψ. Equation 5.3 is consequently called the time-independent Schrödinger equation (the observant reader notices that this equation is of the same form as Eq. 3.1). To get the complete solution to the problem, the wave function obtained by solving Eq. 5.3 is multiplied by the right hand side of Eq. 5.1.

In the present work we solve the time-independent Schrödinger equation by expanding the wave function ψ in a basis set consisting of a series of product wave functions depending on the different coordinates in the Hamiltonian $\hat{H}$. To get an exact solution to Eq. 5.3, the wave function has to be expanded in an infinite set of basis function, resulting in an infinite set of coupled differential equations. This is obviously impossible, and the basis set is always truncated, which is the essence of the close coupling method, developed by Arthurs and Dalgarno in the late fifties [71].

The theory describing the collision between an atom in the ^3P state with a structureless atom, for example a C(^{3}P) or O(^{3}P) atom colliding with an H atom, was developed by Reid [72], Mies [73], and Alexander et a.l. [74]. The Hamiltonian for the scattering problem in Eq. 5.2 can be written as

$$\hat{H} = -\frac{1}{2\mu R}\frac{\partial^2}{\partial R^2}R + \frac{\boldsymbol{l}^2}{2\mu R^2} + V(R) + V_{\mathrm{SO}}, \tag{5.4}$$

where the most important properties of the system are included. Here R is the internuclear distance, μ is the reduced mass of the system, $\boldsymbol{l}$ is the rotational angular momentum of the nuclei, V_{SO} the spin-orbit interaction, and $V(R)$ is the interaction potential between the two atoms. The electronic states of the atoms are specified by the electronic orbital $\boldsymbol{L}$ and spin $\boldsymbol{S}_{\mathrm{O}}$ angular momenta of the oxygen atom and the electronic spin angular momentum $\boldsymbol{S}_{\mathrm{H}}$ of the hydrogen atom. The spin-orbit interaction operator is approximated by the scalar product of the electronic orbital angular momentum $\boldsymbol{L}$ and the electronic spin angular momentum $\boldsymbol{S}$:

$$V_{\mathrm{SO}} = A\boldsymbol{L}\cdot\boldsymbol{S}, \tag{5.5}$$

where the constant A is related to the spin-orbit splitting.

The wave function ψ can be expanded as

$$\psi^{JM} = \frac{1}{R}\sum_{j_{\mathrm{O}}jl} |j_{\mathrm{O}}jlMJ\rangle F^J_{j_{\mathrm{O}}lj}(R), \tag{5.6}$$

where j_O is the total electronic angular momentum of the oxygen atom, j is the total electronic angular momentum of the O-H system, J is the total angular momentum, and M is its space fixed projection.

Substitution of the expansion Eq. 5.6 into the Schrödinger equation, Eq. 5.3, with the Hamiltonian from Eq. 5.4, followed by multiplication from the left by a function $\langle j_{\mathrm{O}} jlMJ|$ and integration over all internal degrees of freedom for the system, results in a set of coupled differential equations

$$\left[\frac{d^2}{dR^2} - \frac{l(l+1)}{R^2} + k_{j_{\mathrm{O}}}^2\right] F_{j_{\mathrm{O}}lj}^J(R) = 2\mu \sum_{j'_{\mathrm{O}}l'j'} V_{j_{\mathrm{O}}lj:j'_{\mathrm{O}}l'j'}^J F_{j'_{\mathrm{O}}l'j'}^J(R). \tag{5.7}$$

The wavenumber $k_{j_{\mathrm{O}}}$ is defined as $k_{j_{\mathrm{O}}}^2 = 2\mu(E - \epsilon_{j_{\mathrm{O}}})$, where E is the total energy of the system and $\epsilon_{j_{\mathrm{O}}}$ is the energy of the fine-structure state j_{O}. Equation 5.7 is a matrix equation, and the aim now is to find the matrix elements $F_{j_{\mathrm{O}}lj}^J(R)$. The matrix element $V_{j_{\mathrm{O}}lj:j'_{\mathrm{O}}l'j'}^J = \langle j_{\mathrm{O}} jlMJ|\hat{V}|j'_{\mathrm{O}} j'l'MJ\rangle$ is evaluated by expanding the interaction potential $V(R)$ as an *effective interaction potential* $v(\boldsymbol{R}, \boldsymbol{r})$ involving only the lone p electron [74],

$$v(\boldsymbol{R}, \boldsymbol{r}) = \sum_{\lambda} V_\lambda(R, r) P_\lambda(\cos\theta). \tag{5.8}$$

Here θ is the angle between the vector $\mathbf{R}$, describing the distance between the two atoms, and the vector $\mathbf{r}$, describing the position of the p electron. After some algebra involving the Legendre polynomials, the expression for the matrix element is obtained [24, 72–75].

The coupled differential equations in Eq. 5.7 are solved by using the log-derivative method [76]. The logarithmic derivative y of the wave function ψ is given by the expression

$$y = \psi'\psi^{-1}. \tag{5.9}$$

This function satisfies the equation

$$y'(R) + W(R) + y^2(R) = 0, \tag{5.10}$$

where $W(R)$ is given by

$$W(R) = k^2 - 2\mu V_{eff}(R, l), \tag{5.11}$$

$$V_{eff} = V(R) + \frac{l(l+1)}{2\mu R^2}. \tag{5.12}$$

Equation 5.10 is numerically integrated using an iterative scheme first described by Johnson [76]. The boundary conditions are as

$$\begin{aligned} &F^J_{j_\mathrm{O} l j; j'_\mathrm{O} l' j'}(R_0) = 0, \\ &F^J_{j_\mathrm{O} l j; j'_\mathrm{O} l' j'}(R \to \infty) = \delta_{j_\mathrm{O} j'_\mathrm{O}} \delta_{j j'} \delta_{l l'} R j_l(k_{j_\mathrm{O}} R) \\ &\quad - K^J_{j_\mathrm{O} l j; j'_\mathrm{O} l' j'} \left(\frac{k_{j_\mathrm{O}}}{k'_{j_\mathrm{O}}} \right)^{1/2} R n_l(k_{j_\mathrm{O}} R) \end{aligned} \tag{5.13}$$

where $\boldsymbol{K}^J$ is a real symmetric matrix, known as the reactance matrix, and j_l and n_j are spherical Bessel functions of the first and second kind. R_0 is chosen sufficiently far inside the classically forbidden region to make the logarithmic derivative y a large but finite value, corresponding to the wave function being arbitrary close to zero.

Solving Eq. 5.10 with the boundary conditions in Eq. 5.13, gives us the reactance matrix $\boldsymbol{K}^J$, from which we can get the useful solution of the scattering problem - the so called scattering matrix $\boldsymbol{S}^J$, containing all the information we need to describe the collision. The scattering matrix $\boldsymbol{S}^J$ is obtained from the $\boldsymbol{K}^J$ matrix through the relation

$$\boldsymbol{S}^J = \left(\mathbf{1} + i\boldsymbol{K}^J\right)\left(\mathbf{1} - i\boldsymbol{K}^J\right)^{-1} \tag{5.14}$$

From the scattering matrix $\boldsymbol{S}^J$ the cross section for the fine-structure transitions is obtained. The partial cross sections $\sigma^J_{j_\mathrm{O} \to j'_\mathrm{O}}$ are given by the expression

$$\sigma^J_{j_\mathrm{O} \to j'_\mathrm{O}}(E) = \frac{\pi}{(2j_\mathrm{O}+1)k^2_{j_\mathrm{O}}} \sum_{j l j' l'} \left| 1 - S^J_{j_\mathrm{O} l j; j'_\mathrm{O} l' j'} \right|^2. \tag{5.15}$$

The cross section for the transitions are obtained by summation over all states:

$$\sigma_{j_\mathrm{O} \to j'_\mathrm{O}}(E) = \sum_J \sigma^J_{j_\mathrm{O} \to j'_\mathrm{O}}(E). \tag{5.16}$$

From the cross sections it is easy to obtain the rate coefficients for the transitions as

$$k_{j_\mathrm{O} \to j'_\mathrm{O}} = \sqrt{\frac{8}{\pi\mu}} (k_B T)^{-3/2} \int_0^\infty \sigma_{j_\mathrm{O} \to j'_\mathrm{O}}(E) E \exp\left(-E/k_B T\right) \mathrm{d}E, \tag{5.17}$$

where k_B is the Boltzman constant.

In this discussion we have only taken into account the ground state of oxygen. If we also include transitions to the first excited electronic state, $\mathrm{O}(^1D)$,

we have to bring the electronic orbital momentum L of oxygen into the expansion, Eq. 5.6, of the wave function. To further complicate the matter, the spin-orbit interaction couples the $L = 1$ and $L = 2$ states of the oxygen atom ($O(^3P)$ and $O(^1D)$, respectively). Thus, L is actually not a good quantum number, and the spin-orbit interaction matrix in the Hamiltonian is not diagonal at $R = \infty$. This can be solved by introducing a transformation matrix in the close coupled equations, and integrate the equations as described by Krems *et al.* [77, 78]

The same methodology outlined here can be used to solve the problem of molecules colliding with atoms, or molecules colliding with molecules. It can also be used to study the reactions between molecules. Of course, the problem will become more complex, as the Hamiltonian in Eq. 5.4 has to contain more terms, such as rotations of the species or interaction with external fields.

5.2 Collisions of ^2P atoms with $^1\Sigma$ molecules

If we exchange the hydrogen in the previous section with a diatomic molecule, not only do we add an extra atom to the system, we also introduce several new physical effects that have to be added to the mathematical description of the problem. In this section we will consider collisions of ^{2}P atoms, such as F(^{2}P), with $^1\Sigma$ molecules, for example $H_2(^1\Sigma)$.

Previously we included the rotation of the system in form of the angular momentum $\boldsymbol{l}$. In addition to that we now also have to include the rotation of the diatomic molecule, represented by the angular momentum $\boldsymbol{j}$ (Note that $\boldsymbol{j}$ is not the same as the quantum number j in Section 5.1). We also have to take into account the electronic potential of the diatom, and its vibrational energy, since the two atoms are free to move with respect to each other along the inter-atomic axis. We also have to consider where the "hole" in the valence shell of the ^2P atom is located with respect to the diatomic molecule, something that complicates the description of the electronic potential.

The theory for time-independent quantum calculations of $X(^2P)$ + $BC(^1\Sigma)$ collisions is based on the work by Baer [79], Rebentrost and Lester [80], Alexander and co-workers [28, 81, 82] and Dubernet and Hutson [83, 84]. In this theory the Hamiltonian describing the collision between $X(^2P)$ atoms with BC diatomic molecules can be written in atomic units as

$$\hat{H}_{tot} = -\frac{1}{2\mu R}\frac{\partial^2}{\partial R^2}R - \frac{1}{2\mu_{\mathrm{BC}}}\frac{\partial^2}{\partial r^2}r + \frac{\boldsymbol{j}^2}{2\mu_{\mathrm{BC}}r^2} + \frac{\boldsymbol{l}^2}{2\mu R^2} + V(r, R, \theta, \theta_a, \phi, \phi_a) + V_{\mathrm{BC}}(r) + \hat{V}_{SO}. \tag{5.18}$$

In this expression, R is the centre-of-mass separation of the colliding particles, r is the interatomic distance in BC, θ and ϕ specify the orientation of the diatomic molecule vector $\boldsymbol{r}$ and θ_a and ϕ_a the orientation of the the hole in the valence shell of the ^2P atom with respect to the atom-molecule separation axis $\boldsymbol{R}$ [83], μ is the reduced mass of the colliding particles and μ_{BC} the reduced mass of the BC molecule. The term V describes the interaction potential of the system, V_{BC} is the intermolecular potential of BC, and $\hat{V}_{SO}$ is the spin-orbital interaction, given by Eq. 5.5. Note that V_{BC} has been subtracted from the interaction potential, something that simplifies the solution of the problem.

The new terms in Eq. 5.18 have to be reflected in the description of the scattered wave. Thus, the scattered wave function is expanded in terms of products of vibrational $\chi_v^j(r)$ and rotational $|jk\rangle$ wave functions of BC, electronic functions $|\mathrm{L}\lambda\mathrm{S}\sigma\rangle$ of the X(^2P) atom, and the Wigner rotation matrix elements:

$$\psi^{JM} = \frac{1}{R}\sqrt{\frac{2J+1}{4\pi}} \sum_{v,j,k,\lambda,\sigma} F^J_{vjkL\lambda S\sigma}(R)\chi_v^j(r) \times D^{J*}_{M,k+\lambda+\sigma}(\alpha_R,\beta_R,0)|jk\rangle|L\lambda S\sigma\rangle. \tag{5.19}$$

Here k, λ, and σ are body-fixed projections of $\boldsymbol{j}$, $\boldsymbol{L}$, and $\boldsymbol{S}$, respectively, on the atom-molecule separation axis, J is the quantum number for the total angular momentum defined as the vector sum of $\boldsymbol{j}$, $\boldsymbol{L}$, $\boldsymbol{S}$, and $\boldsymbol{l}$, and α_R and β_R are the angles describing the orientation of the vector $\boldsymbol{R}$ in the space-fixed coordinate system. $\boldsymbol{L}$ is the electronic orbital angular momentum of the atom.

Using the expansion in Eq. 5.19 to solve the time-independent Schrödinger equation with the Hamiltonian in Eq. 5.18 leads to the following system of coupled differential equations:

$$\left[\frac{d^2}{dR^2} + k_{vj}^2\right] F^J_{vjkL\lambda S\sigma}(R) = 2\mu \sum_{v',j',k',\lambda',\sigma'} \langle vjkL\lambda S\sigma J|\hat{V} + \hat{V}_{\mathrm{SO}} + \frac{\boldsymbol{l}^2}{2\mu R^2}|v'j'k'L\lambda'S\sigma'J\rangle F^J_{v'j'k'L'\lambda'S'\sigma'}(R), \tag{5.20}$$

where $k_{vj}^2 = 2\mu(E-\epsilon_{vj})$, E is the total collision energy and ϵ_{vj} are the ro-vibrational energies of the BC molecule.

The matrix elements $V_{L\lambda S\sigma;L'\lambda'S'\sigma'} = \langle L\lambda S\sigma|\hat{V}|L'\lambda'S'\sigma'\rangle$ can be evaluated as described by Alexander *et al* [28, 81, 82]. This involves a transformation

of the potential from the adiabatic description to a diabatic basis. Once the potential has been transformed, the the full matrix element for the potential can be obtained by numerical integration over the corresponding spherical harmonics using the Gauss-Legendre method [85].

The matrix elements of the spin-orbit and angular momentum operators are obtained through the transformation

$$|j_\mathrm{a}k_\mathrm{a}\rangle = \sum_{\lambda,\sigma} |L\lambda S\sigma\rangle\langle L\lambda S\sigma|j_\mathrm{a}k_\mathrm{a}\rangle \tag{5.21}$$

where j_a is the total electronic angular momentum of the X(^2P) atom ($\boldsymbol{j}_\mathrm{a} = \boldsymbol{L} + \boldsymbol{S}$), k_a is the projection of $\boldsymbol{j}_a$ on the body-fixed quantization axis and the symbol in the brackets is a Clebsch-Gordan coefficient. In the $|j_\mathrm{a}k_\mathrm{a}\rangle$ representation, the spin-orbit Hamiltonian (Eq. 5.5) is diagonal, with the elements corresponding to the energies of the $^2P_{1/2}$ and $^2P_{3/2}$ spin-orbit states of the atom.

The matrix of the $\boldsymbol{l}^2$ operator can be evaluated in the $|jk\rangle|j_\mathrm{a}k_\mathrm{a}\rangle$ basis using the relation:

$$\begin{aligned}\boldsymbol{l}^2 = \boldsymbol{J}^2 + \boldsymbol{j}^2 + \boldsymbol{j}_\mathrm{a}^2 + 2j_{\mathrm{a}z}j_z - 2J_zj_z - 2J_zj_{\mathrm{a}z} + \\ + j_-j_{\mathrm{a}+} + j_+j_{\mathrm{a}-} - J_-j_{\mathrm{a}+} - J_+j_{\mathrm{a}-} - J_-j_+ - J_+j_-,\end{aligned} \tag{5.22}$$

where J_z, $j_{\mathrm{a}z}$ and j_z are the operators that give the z-component of $\boldsymbol{J}$, $\boldsymbol{j}_\mathrm{a}$ and $\boldsymbol{j}$, respectively, and $J_\pm$, $j_{\mathrm{a}\pm}$ and $j_\pm$ are the corresponding ladder operators. The actions of the elements in Eq. 5.22 on the $D^{J*}_{M,k+\lambda+\sigma}|j_ak_a\rangle|jk\rangle$ functions are known [85], and the $\boldsymbol{l}^2$ matrix can be evaluated.

The scattering matrix $S^J_{j_t,l\to j'_t,l'}$ is obtained by solving Eq. 5.20 with the boundary conditions

$$\begin{aligned}&F^J_{vjkL\lambda S\sigma}(R\to 0)\to 0\\ &F^J_{vjkL\lambda S\sigma}(R\to\infty)\sim \delta_{vv'}\delta_{jj'}\delta_{kk'}\delta_{LL'}\delta_{\lambda\lambda'}\delta_{\sigma\sigma'}\exp\left[-i(k_\alpha R-\pi l/2)\right]\\ &\quad - k_\alpha^{-1/2}S^J_{j_t,l\to j'_t,l'}\exp\left[-i(k_\alpha R-\pi l'/2)\right].\end{aligned} \tag{5.23}$$

When the S-matrix is found, the cross section for the electronic and rotational transitions of the X(^2P) + BC collisions are calculated with the relation

$$\begin{aligned}\sigma_{jj_a\to j'j'_a} = &\frac{\pi}{k^2_{j,j_a}(2j_a+1)(2j+1)}\\ &\times\sum_{j_t}\sum_{j'_t}\sum_J(2J+1)\sum_{l,l'}|\delta_{j_t,j'_t}\delta_{l,l'} - S^J_{j_t,l\to j'_t,l'}|^2,\end{aligned} \tag{5.24}$$

where k_{j,j_a} is the wave number of the initial j, j_a state. The first and second summations are performed over all $j_t = j_a + j$ states corresponding to the set of initial and final ro-vibrational levels. From the cross sections, the rate constants are calculated using the relation given in Eq. 5.17.

5.3 Collisions of $^2\Sigma$ molecules with structureless atoms in external fields

Lately the dynamics of molecules in external electric and magnetic fields have been the subject of many studies, both of experimental and theoretical nature. The presence of external fields can dramatically change the dynamics of a collision process. Electrical fields shift and split the electronic levels of a polar molecule into a multiple of states, the so called Stark effect. In the presence of magnetic fields, the Zeeman effect will split the rotational levels, due to interaction between the magnetic field and the magnetic dipole moment associated with the orbital angular momentum. The external fields also couple states characterised by different quantum numbers. The symmetry of the system is completely destroyed if the fields are at an angle with respect to each other, which further complicates the scattering calculations.

The theory for quantum calculations of collisions in magnetic fields was developed by Volpi and Bohn [86] and by Krems and Dalgarno [78]. If the collision is between a structureless atom, such as He, and a polar molecule, only the molecule will be affected by the external fields. Thus, the problem is made somewhat clearer by first discussing the terms in the Hamiltonian for the polar molecule, and then add this Hamiltonian to the Hamiltonian for the full system.

The effects we have to consider for the molecule are the same as in the previous section, such as the rotation of the molecule, the vibrations, and its electronic potential (*c.f.* Eq. 5.18). In addition, we have the effects of the interaction between the electric field and the dipole moment of the molecule, and the interaction between the magnetic field and the spin of the molecule. Since total spin of the molecule is non-zero, we have an interaction between the rotation and the spin, which also has to be included in the Hamiltonian.

Adding all these terms together, we can write the Hamiltonian for a $^2\Sigma$ polar molecule in superimposed electric ($\boldsymbol{E}$) and magnetic ($\boldsymbol{B}$) fields as

$$\hat{H}_{\rm mol} = -\frac{1}{2\mu_m}\frac{d^2}{dr^2} + \frac{\boldsymbol{N}^2(\hat{r})}{2\mu_m r^2} + V(r) + \gamma \boldsymbol{S}\cdot\boldsymbol{N} - \boldsymbol{E}\cdot\boldsymbol{d} + 2\mu_B \boldsymbol{B}\cdot\boldsymbol{S}, \quad (5.25)$$

where μ_m is the reduced mass and $V(r)$ is the potential energy function of the diatomic molecule. The coupling between the rotational ($\boldsymbol{N}$) and spin ($\boldsymbol{S}$) angular momenta is determined by the spin-rotation interaction constant γ, and the coupling between the magnetic field $\boldsymbol{B}$ and the spin is determined by the Bohr magneton μ_B. Here $\hat{r}$ denotes the unit vector in the direction of r.

As only the polar molecule, and not the atom, is affected by the external fields, the total Hamiltonian for the atom-molecule complex will be of the form [78, 86]

$$\hat{H} = -\frac{1}{2\mu R}\frac{d^2}{dR^2}R + \frac{\boldsymbol{\ell}^2}{2\mu R^2} + V(R, r, \theta) + \hat{H}_{\rm mol}, \tag{5.26}$$

where μ is the reduced mass of the collision, and R is the distance between the center of mass of the diatomic molecule and the atom. $\boldsymbol{\ell}$ is the orbital angular momentum for the collision (*c.f.* Eq. 5.18), and $H_{\rm mol}$ is the molecular Hamiltonian from Eq. 5.25.

The scattering wave function is expanded in a fully uncoupled set of space-fixed basis functions

$$|NM_N\rangle|SM_S\rangle|\ell M_\ell\rangle, \tag{5.27}$$

where M_N, M_S, and M_ℓ denote the projections of $\boldsymbol{N}$, $\boldsymbol{S}$, and $\boldsymbol{\ell}$ on the magnetic field axis [78]. When the electric and magnetic fields are parallel or antiparallel, the projection of the total angular momentum $M = M_N + M_S + M_\ell$ is conserved, and the scattering calculations can be carried out in a cycle over M [47, 78]. If the electric and magnetic fields are rotated, the electric field couples states with different M_N, and the projection of the total angular momentum M is no longer a good quantum number. The R-dependent expansion coefficients $F_{NM_NSM_S\ell M_\ell}(R)$ of the total wave function in the basis set (5.27) are obtained by solving a set of close-coupled equations [48, 78]

$$\begin{aligned}\left[\frac{d^2}{dR^2} + 2\mu E_{\rm tot} - \frac{\ell(\ell+1)}{R^2}\right] F_{NM_NSM_S\ell M_\ell}(R) \\ = 2\mu \sum_{N', M'_N, S, M'_S, \ell', M'_\ell} \langle NM_NSM_S\ell M_\ell|V(R, r, \theta) + \\ H_{\rm mol}|N'M'_NSM'_S\ell' M'_\ell\rangle F_{N'M'_NSM'_S\ell' M'_\ell}(R),\end{aligned} \tag{5.28}$$

where $E_{\rm tot}$ is the total energy of the system.

To solve Eq. 5.28 numerically, the different terms have to be rewritten in their matrix form, in the same manner as outlined in the previous sections. The interaction of the electron spin with the magnetic field $\boldsymbol{B}$ is given by $2\mu_B \boldsymbol{B}\cdot\boldsymbol{S}$, where μ_B is the Bohr magneton. If the space fixed quantization axis Z is oriented along the magnetic field direction only the Z-component of the vector $\boldsymbol{B}$ is nonzero and the last term in Eq. (5.25) reduces to $2\mu_B B S_Z$. The expression for the rotational angular momentum $\boldsymbol{N}$ is given by the relation

$$\frac{\boldsymbol{N}^2}{r^2} = \frac{N(N+1)}{r^2}, \tag{5.29}$$

and the coupling between the rotational ($\boldsymbol{N}$) and spin ($\boldsymbol{S}$) angular momenta is given by the expression

$$\gamma \boldsymbol{N} \cdot \boldsymbol{S} = \gamma(N_z S_z + \frac{1}{2}(N_+ S_- + N_- S_+)), \tag{5.30}$$

where $N_\pm$ and $S_\pm$ are the lowering and raising operators, given by $N_\pm = N_x \pm iN_y$ and $S_\pm = S_x \pm iS_y$, respectively [85].

The interaction potential $V(R, r, \theta)$ couples different rotational states, and is thus not diagonal the expansion in Eq. 5.27. By expanding V in spherical harmonics

$$\begin{aligned} V(R, r, \theta) = &\sum_\lambda \left(\frac{4\pi}{2\lambda + 1} \right) V_\lambda(R, r) \\ &\times \sum_{m_\lambda} (-1)^{m_\lambda} Y_{\lambda, -m_\lambda}(\hat{R}) Y_{\lambda, m_\lambda}(\hat{R}) \end{aligned} \tag{5.31}$$

the matrix element of V can be evaluated using the Wigner-Eckart theorem [85]. $\hat{R}$ and $\hat{r}$ in Eq. 5.31 are unit vectors in the direction of $\mathbf{R}$ and $\mathbf{r}$, respectively. The matrix element for V is then given by the expression

$$\begin{aligned} &\langle N M_N | \langle S M_S \langle \ell M_\ell | V(R, r, \theta) | N' M'_N \rangle | S M'_S \rangle | \ell' M'_\ell \rangle \\ &= \delta_{M_S M'_S} \sum_\lambda V_\lambda(R, r) \begin{pmatrix} \ell & \lambda & \ell' \\ 0 & 0 & 0 \end{pmatrix} \begin{pmatrix} N' & \lambda & N' \\ 0 & 0 & 0 \end{pmatrix} \\ &\times [(2\ell + 1)(2\ell' + 1)(2N + 1)(2N' + 1)]^{1/2} \\ &\times \sum_{m_\lambda} (-1)^{m_\lambda} (-1)^{m_\ell} (-1)^{m_N} \\ &\times \begin{pmatrix} \ell & \lambda & \ell' \\ -m_\ell & -m_\lambda & m'_\ell \end{pmatrix} \begin{pmatrix} N' & \lambda & N' \\ -M_N & m_\lambda & M_N \end{pmatrix}, \end{aligned} \tag{5.32}$$

where the symbols in parentheses are 3–j symbols [78, 85].

The interaction with electric fields can be written as $-\boldsymbol{E} \cdot \boldsymbol{d} = -Ed \cos\chi$, where χ is the angle between the electric field direction $\hat{E}$ and the molecular axis $\hat{r}$, E is the electric field strength and d is the electric dipole moment of the molecule. Using the spherical harmonic addition theorem [85], this term can be rewritten as a sum over products of spherical harmonics

$$-Ed \cos\chi = -Ed \frac{4\pi}{3} \sum_q Y^*_{1q}(\hat{r}) Y_{1q}(\hat{E}). \tag{5.33}$$

The matrix of the interaction with electric fields (5.33) will then be given by

$$\begin{aligned} &\langle N M_N | - Ed \cos\chi | N' M'_N \rangle \\ &= -Ed \frac{4\pi}{3} \sum_q Y_{1q}(\hat{E}) \langle N M_N | Y^*_{1q}(\hat{r}) | N' M'_N \rangle, \end{aligned} \tag{5.34}$$

and is diagonal in the S, M_S, ℓ, and M_ℓ quantum numbers. The evaluation of the integrals in Eq. (5.34) provides a general expression for the matrix elements of the interaction with electric fields of arbitrary orientation,

$$\begin{aligned}\langle N M_N S M_S \ell M_\ell | - Ed\cos\chi \, | N' M'_N S' M'_S \ell' M'_\ell \rangle \\ = -\delta_{\ell'\ell}\,\delta_{M'_\ell M_\ell}\delta_{M'_S M_S} Ed (-1)^{M_N} Y_{1,M'_N - M_N}(\hat{E}) \left[(2N+1)(2N'+1)\right]^{1/2} \\ \times \begin{pmatrix} N' & 1 & N \\ 0 & 0 & 0 \end{pmatrix} \begin{pmatrix} N' & 1 & N \\ M'_N & M_N - M'_N & -M_N \end{pmatrix},\end{aligned} \tag{5.35}$$

where the symbols in parentheses are 3–j symbols [85].

When the magnetic and electric fields are both oriented along the Z-axis, the spherical harmonics $Y_{1q}(\hat{E})$ in Eq. (5.34) reduce to

$$Y_{1q} = \left(\frac{3}{4\pi}\right)^{1/2} \delta_{q0}, \tag{5.36}$$

which, inserted in Eq. (5.33), gives

$$-Ed\cos\chi = -Ed\left(\frac{4\pi}{3}\right)^{1/2} Y_{10}(\hat{r}). \tag{5.37}$$

For parallel fields, $q = M'_N - M_N = 0$, and Eq. (5.35) is reduced to the expression [48]

$$\begin{aligned}\langle N M_N S M_S \ell M_\ell | - Ed\cos\chi \, | N' M'_N S' M'_S \ell' M'_\ell \rangle \\ = -\delta_{\ell'\ell}\,\delta_{M'_\ell M_\ell}\delta_{M'_S M_S}\delta_{M'_N M_N} Ed (-1)^{M_N} \left[(2N+1)(2N'+1)\right]^{1/2} \\ \times \begin{pmatrix} N' & 1 & N \\ 0 & 0 & 0 \end{pmatrix} \begin{pmatrix} N' & 1 & N \\ -M_N & 0 & M_N \end{pmatrix}.\end{aligned} \tag{5.38}$$

When all matrix elements are derived, the close coupled equations (Eq. 5.28) are solved with the boundary conditions from Eq. 5.23. From the scattering matrix S the cross sections are calculated, which gives us the rate constants, using the relationship given in Eq. 5.17.

This theory can be expanded to include the collisions of $^2\Sigma$ molecules with ^{2}S atoms, or collisions of two $^2\Sigma$ molecules. Both these species can be trapped by the magnetic field, and the reactions can directly be observed by monitoring the trap loss [87, 88]. This propose that reactions of open-shell molecules may be effectively controlled at low temperatures by electric fields, which is a very interesting prospect.

Chapter 6

Results and Conclusions

My work has reached over several chemical systems, and different methods. In the following section my research is summarized, and a few conclusions are drawn.

6.1 Results

The results of my research efforts are presented and discussed in detail in the attached research papers. In the following section a short summary of each of the papers is given, giving the reader an introduction to my findings.

6.1.1 Paper I

In Paper I we present CASPT2 calculations on the lowest collinear $^2\Pi$ and $^4\Sigma^-$ potential energy surfaces for the CNO system, corresponding to the $O + CN \rightarrow N + CO$ reaction. The potential energy surfaces are interpolated using the GDVR method. Both surfaces are exothermic, with an energy difference of 0.81 eV for the $^2\Pi$ and 3.39 eV for the $^4\Sigma^-$ surface. While the $^2\Pi$ surface has a 5.85 eV deep potential well and no barrier, the $^4\Sigma^-$ surface exhibits a potential barrier of 1.42 eV and no well.

Time-dependent wave packet calculations using the split-operator propagator have been performed on both surfaces in product Jacobi coordinates. The results on the $^2\Pi$ surface show structure in the reaction probabilities as a function of energy up to about 0.5 eV translational energy. On the $^4\Sigma^-$ surface the reaction is highly vibrationally non-adiabatic with initial translational energy more efficient in promoting the reaction than initial vi-

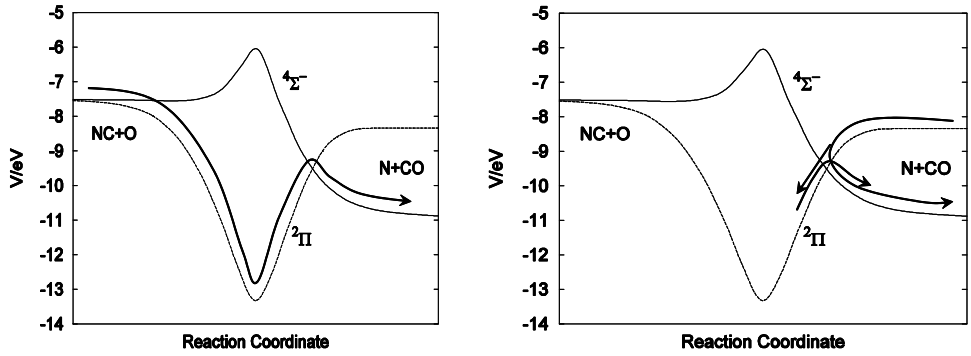

Figure 6.1: Possible pathways for transition from the $^2\Pi$ to the $^4\Sigma^-$ surface for the $O + CN \rightarrow N + CO$ reaction (left) and the non-reactive scattering of N+CO (right)

brational excitation. For reaction out of $v = 0$ the wave packet results show a systematic trend of increasing reaction probabilities for increasing product vibrational excitation up to $v' = 3$, thereafter the reaction probabilities decrease with further increasing product vibrational excitation. For reaction out of $v = 1$ and $v = 2$ these systematic trends are not observed. The wave packet calculations are compared to quasiclassical trajectory calculations. Generally the agreement is good, as would be expected, as the atoms are relatively heavy. Differences in the product vibrational distributions primarily appear from reaction out of $v = 0$, which is related to the significant difference in initial classical and quantum distributions for $v = 0$.

6.1.2 Paper II

In Paper II spin-orbit coupling between the two collinear $^2\Pi$ and $^4\Sigma^-$ potential energy surfaces for the CNO system are presented. The spin-orbit couplings are calculated using the RASSI method with CASSCF wave functions as basis set. The full spin-orbit coupling surface is interpolated using the GDVR method. The spin-orbit coupling is the strongest in the O + CN configuration, reaching a maximum of 0.007 eV before the crossing of the two potential energy surfaces. At the crossing the spin-orbit coupling is about 0.004 eV.

Wave packet calculations and TSH calculations on the coupled surfaces are presented for both the $O + CN \rightarrow N + CO$ reaction and the non-reactive scattering process $N + CO \rightarrow N + CO$. The two cases are shown in Fig. 6.1, where possible adiabatic pathways are illustrated by arrows.

In the former case, O + CN can react and form ground state CO and nitrogen in either the ground state ($N(^4S)$) or in the first excited state ($N(^2D)$). The energies studied are considerably lower than the potential energy barrier on the $^4\Sigma^-$ surface. Thus, all reactive processes have to enter the potential well of the $^2\Pi$ surface. After the potential well, the two surfaces cross, and spin-orbit coupling can allow transitions between the surfaces. Both the wave packet and the TSH calculations show that this probability is low, about 0.05%, and has weak energy dependence, with slightly higher transition probabilities at lower energies.

The non-reactive scattering process N + CO → N + CO is initiated in the $N(^2D)$ + CO channel on the $^2\Pi$ surface with kinetic energies below 0.7 eV, to avoid the formation of CN + O. The system can either stay on the diabatic $^2\Pi$ surface, returning to the $N(^2D)$ + CO state, or it can transfer to the $^4\Sigma^-$ surface, and exit in the ground state $N(^4S)$ + CO channel. The TSH calculations show strong energy dependence in the transition probabilities. For energies below approximately 0.35 eV, the probability of crossing over to the lower diabatic surface, producing ground state nitrogen, is over 15%, while higher energies only allows the creation of a few percent ground state nitrogen. The wave packet calculations result in an average probability of around 0.5%. However, the transition probability shows a distinct resonance pattern, with peaks reaching a transition probability of about 10%. The wave packet calculations also show energy dependence in the transition probability, with larger peaks at lower energies, thus following the trend of the TSH calculations.

6.1.3 Paper III

Using accurate interaction potentials, we performed refined calculations of rate coefficients for the fine-structure exitation of $O(^3P)$ and $C(^3P)$ with atomic hydrogen, using time-independent quantum dynamics. The spin-orbit interaction splits the ground electronic states of oxygen and carbon into a triplet of fine-structure levels $^3P_0$, $^3P_1$, and $^3P_2$. The lowest state for oxygen is $^3P_2$ and that of carbon is $^3P_0$.

We found significant disagreement between the rate coefficients calculated in the present work and the previous results [24]. We showed that the rate coefficients are very sensitive to variations in the short-range interaction potentials. We also included the coupling between the $O(^3P)$ and $O(^1D)$ states in our calculations. It showed that the coupling to the ^1D state appear to be insignificant even at collision energies up to 10 000 cm^{-1}.

6.1.4 Paper IV

We present quantum scattering calculations of rate coefficients for the spin-orbit relaxation of F($^2P_{1/2}$) atoms in a gas of H_2 molecules and Cl($^2P_{1/2}$) atoms in a gas of H_2 and D_2 molecules. The spin-orbit interaction in the ground electronic state of the halogen atoms gives rise to two fine structure energy levels $^2P_{1/2}$ and $^2P_{3/2}$. The interactions of F(^2P) and Cl(^2P) with H_2 are characterized by three adiabatic interaction potentials and the reactions of F($^2P_{1/2}$) and Cl($^2P_{1/2}$) with H_2 occur at low temperatures through non-adiabatic transitions [30]. The same interactions determine the dynamics of spin-orbit transitions in non-reactive collisions of halogen atoms with H_2. The analysis of fine structure relaxation in pre-reactive F(^2P) - H_2 and Cl(^2P) - H_2 complexes may therefore elucidate the mechanisms of the chemical reactions and help resolve the disagreements with experiments. Rigorous quantum mechanical calculations demonstrated that the spin-orbit relaxation in F($^2P_{1/2}$) + H_2 collisions is dominated by near-resonant energy transfer [31, 80].

Our calculation of the thermally averaged rate coefficient for the electronic relaxation of chlorine in H_2 agrees with an experimental measurement at room temperature. This finding suggests that the interaction potential calculated by Klos *et. al.* [89] is accurate for the simulation of nonadiabatic dynamics in the entrance channel of the Cl(^2P) + H_2 reaction. We found that the spin-orbit relaxation of chlorine atoms in collisions with hydrogen molecules in the rotationally excited state $j = 2$ is dominated by near-resonant electronic-to-rotational energy transfer accompanied by rotational excitation of the molecules. The rate of the spin-orbit relaxation in collisions with D_2 molecules increases to a great extent with the rotational excitation of the molecules. We have found that the H_2/D_2 isotope effect in the relaxation of Cl($^2P_{1/2}$) is very sensitive to temperature due to the significant role of molecular rotations in the non-adiabatic transitions. Our calculation yields a rate ratio of 10 for the electronic relaxation of chlorine in H_2 and D_2 gases at room temperature, in qualitative agreement with the experimental measurement of the isotope ratio of about 5. The isotope effect becomes less significant at higher temperatures.

6.1.5 Paper V

We present a detailed study of low-temperature collisions between CaD($^2\Sigma$) molecules and He atoms in superimposed electric and magnetic fields with arbitrary orientations. Electric fields do not interact with the electron spin of the molecules directly, but modify their rotational structure and, consequently, the spin-rotation interactions. We examine the molecular Stark

and Zeeman energy levels as functions of the angle between the fields and show that rotating fields may induce and shift avoided crossings between the Zeeman levels of the rotationally ground and rotationally excited states of the molecule. Inelastic Zeeman transitions in collisions of molecules may therefore be effectively controlled by varying the strength and the relative orientation of the applied fields near the avoided crossings.

We have reported calculations of rate constants for rotationally inelastic collisions of CaD molecules at temperatures up to 60 K. Our results show that molecular collisions can be sensitive to electric fields even at relatively high temperatures (10 K). We demonstrate that external fields modify the resonance structure of the cross sections at collision energies up to 60 K and show that electric fields may induce forbidden transitions in atom-molecule scattering at ultracold temperatures. The wide range of temperatures we considered in this work is experimentally accessible and our results can be tested in a variety of experiments with cold molecules. This is the first reported theoretical study of collisions of molecules in electric and magnetic fields at arbitrary angles.

6.1.6 Paper VI

In Paper VI we once again return to the CNO system. We have discovered new reaction paths from $C(^3P) + NO(X^2\Pi)$ to $CN(X^2\Sigma^+) + O(^3P)$ and $CO(X^1\Sigma^+) + N(^4S)$ without significant barriers. High level CASPT2 calculations were performed for the two lowest $^4A''$ surfaces for the CNO system. The higher surface has significant barriers to reaction, and was not further studied, while the lower showed no barriers against reaction. The lowest of the two surfaces was fitted to an analytic expression using a many-body expansion.

Quasiclassical trajectory calculations were carried out on the lowest $^4A''$ surface at temperatures between 10 and 4000 K. We also performed QCT calculations simulating crossed molecular beam experiments of the $C(^3P) + NO(X^2\Pi) \rightarrow CN(X^2\Sigma^+) + O(^3P)$ reaction. The results were combined with the results from our previous work and compared with experiments. The results from our calculations show very good agreement with experiments, and indicate that the $^4A''$ surface is of great importance for the dynamics of the CNO system.

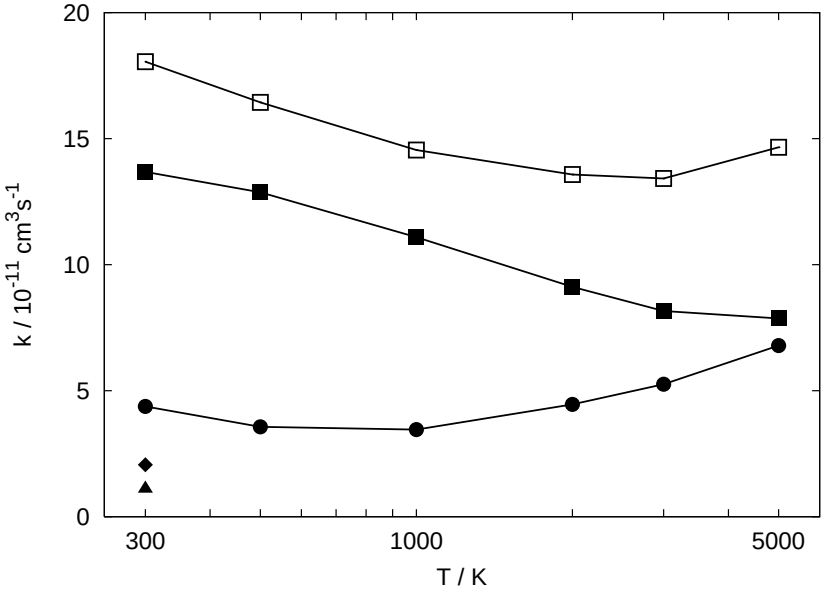

Figure 6.2: Thermal rate coefficients for the $O + CN \rightarrow N + CO$ reaction; total rate coefficients for the reaction on the $^2A'$, $^2A''$, and $^4A''$ surfaces using Fit 1 of the $^4A''$ surfaces (unfilled squares); rate coefficients for the $^2A'$ and $^2A''$ surfaces (filled squares); rate coefficients for the $^4A''$ surface using Fit 1 (filled circles), Fit 2 (filled triangle), and Fit 3 (filled diamond).

6.2 Work in progress

We have performed quasiclassical trajectory calculations for the O + CN → N + CO reaction on the lowest $^4A''$ surface, calculated in Paper VI. However, the current fit to the analytical expansion is not sufficiently accurate to allow for quantitative calculations of the rate coefficients for the reaction. We have calculated the rate coefficients for the reaction using three different fits, of similar accuracy, reaching very different results (see Fig. 6.2). The total rate coefficients are calculated combining the rate coefficients on the $^2A'$, $^2A''$ (from Ref. [5]), and $^4A''$ surfaces. Compared to the experimental rate coefficients listed in Tab. 6.1, it is clear that the calculations are in disagreement with the experiments at room temperature, but in good agreement above 3000 K. However, if we compare the calculated rate coefficients from the doublet surfaces and the $^4A''$ surface, we see that we can draw the qualitative conclusion that the inclusion of the $^4A''$ surface can at least partly explain the 20% groundstate nitrogen found in experiments from the O + CN reaction.

Table 6.1: Thermal rate coefficients for the O + CN reaction.

	T/K	$k/10^{-11}$ cm^{3}s^{-1}
Schmatjko and Wolfrum [17]	298	1.7 ± 0.7
Titarchuk and Halpern [90]	298	3.69 ± 0.75
Boden and Thrush [91]	570–687	$(10.5 \pm 5.8)\ \exp[(-1200 \pm 350)/T]$
Louge and Hanson [92]	2000	3.0 + 2.6/-1.3
Davidson *et al.* [93]	3000–4500	13.0 ± 2.6

6.3 Conclusions

- It has been shown that small but noticeable quantum effects are seen for the collinear O + CN → N + CO reaction on the $^2\Pi$ and $^4\Sigma^-$ surfaces.

- The experimental detection of N(^{4}S) in the O + CN → N + CO reaction cannot be explained by collinear reaction on the $^2\Pi$ and $^4\Sigma^-$ surfaces. It has furthermore been shown that spin-orbit interaction between the collinear surfaces is too weak to explain the production of N(^{4}S).

- A new potential energy surface, ^{4}A″, for the CNO system has been presented. This surface shows a previously undiscovered reaction path without significant barrier from C(^{3}P) + NO(X$^2\Pi$) to CN(X$^2\Sigma^+$) + O(^{3}P) and CO(X$^1\Sigma^+$) + N(^{4}S). Inclusion of the ^{4}A″ surface in the calculations of the rate coefficients for the C + NO reaction significantly improves the agreement with experiments.

- The ^{4}A″ surface might explain the production of N(^{4}S) for the O + CN → N + CO reaction, as it has a reaction path to N(^{4}S) without significant barriers.

- Improved calculations of the rate constants for fine-structure excitation of O I and C I in collisions with H have been presented. It was shown that the coupling between the O(^{3}P) and O(^{1}D) states is insignificant even for very high collision energies.

- The obtained results for the spin-orbit relaxation of Cl(^{2}P) and F(^{2}P) in a gas of H_2 supports the findings of previous calculations.

- The first report of spin-orbit relaxation of polar molecules in combined electric and magnetic fields has been presented. It was show that the spin-orbit relaxation can be controlled by the strengths of the fields, as well as the angle between them, at temperatures easily obtainable in experiments.

Chapter 7

Future and Outlook

Even though the CNO system has been under investigations for decades (the earliest work in our group is from 1995 [1]), there are still many aspects of this system that are still to be investigated. The combination of three heavy atoms and a deep potential well makes the system very interesting, and wave packet calculations with full dimensionality nearly impossible to perform.

Previous 2D wave packet calculations, both by us and other groups, have shown that there are quantum effects present, even for the heavy CNO system, in the collinear configuration. It would be very interesting to perform full dimensional wave packet calculations on the available 3D surfaces and compare the result with the collinear and classical studies.

In this and previous studies of the CNO system, the Renner-Teller effects have been neglected. The Born-Oppenheimer approximation breaks down due to the degenerate ground states, and it is possible that these effects would affect the dynamics of the system, by allowing intersurface crossing.

There are several excited states of the CNO system that have not been investigated. We believe that there could be at least one additional surface that might be accessible for C + NO $\rightarrow$ O + CN reaction. Non-adiabatic processes, such as spin-orbit coupling, could facilitate reaction pathways previously undiscovered. The first task would be the calculations of other excited states, followed by the study of the couplings between the different surfaces.

The discrepancy between experiment and theory for the Cl + H_2 reaction needs to be further investigated. Mostly, experimental efforts to prove or disprove the near-resonant energy transfer of the spin-orbit relaxation for both F($^2P_{1/2}$) and Cl($^2P_{1/2}$) are needed to provide more insight into the mechanisms of the electronic relaxation.

The work on dynamics of molecules in crossed electric and magnetic fields has only begun. The theory on collisions between $^2\Sigma$ molecules and ^2S atoms needs to be evaluated with scattering calculations and compared to experiments. The theory furthermore needs to be expanded to collisions between molecules and atoms of other symmetries.

Bibliography

[1] B. J. Persson, B. O. Roos, and M. Simonson, *Chem. Phys. Lett.*, 1995, **234**, 382.

[2] M. Simonson, N. Marković, S. Nordholm, and B. Persson, *Chem. Phys.*, 1995, **200**, 141.

[3] S. Andersson, N. Marković, and G. Nyman, *Phys. Chem. Chem. Phys.*, 2000, **2**, 613.

[4] S. Andersson, N. Marković, and G. Nyman, *Chem. Phys.*, 2000, **259**, 99.

[5] S. Andersson, N. Marković, and G. Nyman, *J. Phys. Chem.*, 2003, **107**, 5439.

[6] E. Herbst and W. Klemperer, *Astrophys. J.*, 1973, **185**, 505.

[7] E. Herbst, H.-H. Lee, D. Howe, and T. Millar, *Mon. Not. R. Astron. Soc.*, 1994, **268**, 335.

[8] G. D. Forêtes, E. Roueff, and D. Flower, *Mon. Not. R. Astron. Soc.*, 1990, **244**, 668.

[9] S. Federman, C. Strom, D. Lambert, J. Cardelli, V. Smith, and C. Joseph, *Astrophys. J.*, 1994, **424**, 772.

[10] M. Gerin, Y. Viala, F. Pauzat, and Y. Elliinger, *Astron. Astrophys.*, 1992, **266**, 463.

[11] G. I. Borger and A. Sternberg, *ApJ*, 2005, **632**, 302.

[12] M. Monnerville, P. Halvick, and J. Rayez, *J. Chem. Soc. Faraday Trans.*, 1993, **89**, 1579.

[13] M. Monnerville, G. Peoux, S. Briquez, and P. Halvick, *Chem. Phys. Lett.*, 2000, **322**, 157.

[14] A. Abrol, L. Wiesenfeld, B. Lambert, and A. Kuppermann, *J. Chem. Phys.*, 2001, **114**, 7461.

[15] C. Schulz, H.-R. Volpp, and J. Wolfrum in *Chemical Dynamics in Extreme Environments*, ed. R. Dressler; World Scientiffic, Singapore, 2001; p. 206.

[16] K. J. Schmatjko and J. Wolfrum, *J. Ber. Bunsenges. Phys. Chem.*, 1975, **79**, 696.

[17] K. J. Schmatjko and J. Wolfrum, *J. Ber. Bunsenges. Phys. Chem.*, 1978, **82**, 419.

[18] C. J. Cobos, *React. Kinet. Catal. Lett.*, 1996, **57**, 43.

[19] R. V. Krems, *Int. Rev. Phys. Chem.*, 2005, **24**, 99.

[20] A. Dalgarno and R. A. McCray, *Ann. Rev. Astron. Astrophys.*, 1972, **10**, 375.

[21] L. L. Cowie and A. Songaila, *Ann. Rev. Astron. Astrophys.*, 1986, **24**, 499.

[22] R. Quast, R. Baade, and D. Reimers, *Astron. Astrophys.*, 2002, **386**, 796.

[23] G. Shaw, G. J. Ferland, R. Srianand, and N. P. Abel, *ApJ*, 2006, **639**, 941.

[24] J.-M. Launay and E. Roueff, *A&A*, 1977, **56**, 289.

[25] D. R. Yarkony, *J. Chem. Phys.*, 1992, **97**, 1838.

[26] G. Parlant and D. R. Yarkony, *J. Chem. Phys.*, 1999, **110**, 363.

[27] A. Kalemos, A. Mavridis, and A. Metropoulos, *J. Chem. Phys.*, 1999, **111**, 9536.

[28] M. H. Alexander, D. E. Manolopoulos, and H.-J. Werner, *J. Chem. Phys.*, 2000, **113**, 11084.

[29] J. Kłos, M. M. Szczęśniak, and G. Chałasiński, *Int. Rev. Phys. Chem*, 2004, **23**, 541.

[30] M. H. Alexander, G. Capecchi, and H.-J. Werner, *Science*, 2002, **296**, 715.

[31] C. Zhu, R. Krems, A. Dalgarno, and N. Balakrishnan, *ApJ*, 2002, **577**, 795.

[32] S.-H. Lee and K. Liu, *J. Chem. Phys.*, 1999, **111**, 6253.

[33] S.-H. Lee, L.-H. Lai, K. Liu, and H. Chang, *J. Chem. Phys.*, 1999, **110**, 8229.

[34] F. Dong, S.-H. Lee, and K. Liu, *J. Chem. Phys.*, 2001, **115**, 1197.

[35] H. Stapelfeldt and T. Seideman, *Rev. Mod. Phys.*, 2003, **75**, 543.

[36] V. Aquilanti, D. Ascenzi, D. Cappelletti, and F. Pirani, *Nature (London)*, 1994, **371**, 399.

[37] D. Cappelletti, A. Gerbi, F. Pirani, M. Rocca, M. Scotoni, L. Vattuone, and U. Valbusa, *Phys. Scr.*, 2006, **C73**, 20.

[38] V. Aquilanti, D. Ascenzi, D. Cappelletti, S. Franceschini, and F. Pirani, *Phys. Rev. Lett.*, 1995, **74**, 2929.

[39] R. J. Levis, G. Menkir, and H. Rabitz, *Science*, 2001, **292**, 709.

[40] J. Itatani, J. Levesque, D. Zeidler, H. Niikura, H. Pépin, J. C. Kieffer, P. B. Corkum, and D. M. Villeneuve, *Nature (London)*, 2004, **432**, 867.

[41] H. Stapelfeldt, *Nature (London)*, 2004, **432**, 809.

[42] C. E. Heiner, D. Carty, G. Meijer, and H. L. Bethlem, *Nat. Phys.*, 2007, **3**, 115.

[43] R. V. Krems, *Nat. Phys.*, 2007, **3**, 77.

[44] A. L. Migdall, J. V. Prodan, W. D. Phillips, T. H. Bergeman, and H. J. Metcalf, *Phys. Rev. Lett.*, 1985, **54**, 2596.

[45] J. M. Doyle, B. Friedrich, J. Kim, and D. Patterson, *Phys. Rev. A*, 1995, **52**, R2515.

[46] J. Doyle, B. Friedrich, R. V. Krems, and F. Masnou-Seeuws, *Eur. Phys. J. D*, 2004, **31**, 149.

[47] T. V. Tscherbul and R. V. Krems, *Phys. Rev. Lett.*, 2006, **97**, 083201.

[48] T. V. Tscherbul and R. V. Krems, *J. Chem. Phys.*, 2006, **125**, 194311.

[49] T. Helgaker, P. Jørgensen, and J. Olsen, *Molecular Electronic-Structure Theory*, Wiley, Chichester, 2000.

[50] C. Møller and M. S. Plesset, *Phys. Rev.*, 1934, **48**, 618.

[51] C. J. Cramer, *Essentials of Computational Chemistry*, Wiley, Chichester, 2002.

[52] B. O. Roos, *Chem. Phys.*, 1982, **66**, 197.

[53] S. Sato, *J. Chem. Phys.*, 1955, **23**, 592.

[54] J. Murrell, S. Carter, S. Farantos, P. Huxley, and A. Varandas, *Molecular Potential Energy Surfaces*, Wiley, Chichester, 1984.

[55] G. Nyman and H.-G. Yu, *Rep. Prog. Phys.*, 2000, **63**, 1001.

[56] H. G. Yu, S. Andersson, and G. Nyman, *Chem. Phys. Lett.*, 2000, **321**, 275.

[57] H. G. Yu and G. Nyman, *J. Chem. Phys.*, 2000, **113**, 8936.

[58] H.-G. Yu and G. Nyman, *J. Chem. Phys.*, 2001, **105**, 2240.

[59] H.-G. Yu, T. Gonzales-Lezana, A. Marr, J. Muckerman, and T. Sears, *J. Chem. Phys.*, 2001, **115**, 5433.

[60] A. Aguado and M. Paniagua, *J. Chem. Phys.*, 1992, **96**, 1265.

[61] J. Sakurai, *Modern Quantum Mechanics Rev.Ed.*, Addison Wesley, Reading, 1994.

[62] L. M. Raff and D. L. Thompson in *Theory of Chemical Reaction Dynamics, Volume III*, ed. M. Baer; CRC Press, Boca Raton, 1985.

[63] F. J. Aoiz, L. Bañares, and V. J. Herrero, *J. Chem. Soc. Faraday Trans.*, 1998, **94**, 2483.

[64] J. Stine and J. Muckerman, *J. Chem. Phys.*, 1976, **65**, 3975.

[65] J. Stine and J. Muckerman, *J. Chem. Phys.*, 1978, **68**, 185.

[66] R. Preston and J. Tully, *J. Chem. Phys.*, 1971, **54**, 4297.

[67] C. Leforestier, R. H. Bisseling, C. Cerjan, M. D. Feit, R. Friesner, A. Guldberg, A. Hammerich, G. Jolicard, W. Karrlein, H. D. Meyer, N. Lipkin, O. Roncero, and R. Kosloff, *J. Comput. Phys.*, 1991, **94**, 59.

[68] D. Kosloff and R. Kosloff, *Comput. Phys. Letters*, 1983, **173**, 35.

[69] Á. Vibók and G. G. Balint-Kurti, *J. Phys. Chem.*, 1992, **96**, 8712.

[70] N. Marković and G. D. Billing, *J. Chem. Phys.*, 1994, **100**, 1085.

[71] A. Arthurs and A. Dalgarno, *Proc. R. Soc. London, Ser. A*, 1960, **256**, 540.

[72] R. H. G. Reid, *J. Phys. B: Atom. Molec. Phys.*, 1973, **6**, 2018.

[73] F. H. Mies, *Phys. Rev. A*, 1973, **7**, 942.

[74] M. H. Alexander, T. Orlikowski, and J. E. Straub, *Phys. Rev. A*, 1983, **28**, 73.

[75] J. C. Weisheit and N. F. Lane, *Phys. Rev. A*, 1971, **4**, 171.

[76] B. R. Johnson, *J. Comput. Phys.*, 1973, **13**, 445.

[77] R. V. Krems, M. J. Jamieson, and A. Dalgarno, *Astrophys. J*, 2006, **647**, 1531.

[78] R. V. Krems and A. Dalgarno, *J. Chem. Phys.*, 2004, **120**, 2296.

[79] M. Baer, *Chem. Phys. Lett.*, 1975, **35**, 112.

[80] F. Rebenrost and W. A. Lester, Jr., *J. Chem. Phys.*, 1976, **64**, 3879.

[81] M. H. Alexander, *J. Chem. Phys.*, 1993, **99**, 6014.

[82] M. H. Alexander and M. Yang, *J. Chem. Phys.*, 1995, **103**, 7956.

[83] M.-L. Dubernet and J. M. Hutson, *J. Chem. Phys.*, 1994, **101**, 1939.

[84] M.-L. Dubernet and J. M. Hutson, *J. Phys. Chem.*, 1994, **98**, 5844.

[85] R. N. Zare, *Angular Momentum*, Wiley, New York, 1988.

[86] A. Volpi and L. Bohn, *Phys. Rev. A*, 2002, **65**, 052712.

[87] P. Staanum, S. D. Kraft, J. Lange, R. Wester, and M. Weidemüller, *Phys. Rev. Lett.*, 2006, **96**, 023201.

[88] N. Zahzam, T. Vogt, M. Mudrich, D. Comparat, and P. Pillet, *Phys. Rev. Lett.*, 2006, **96**, 023202.

[89] J. Kłos, G. Chałasiński, and M. M. Szczęśniak, *J. Chem. Phys.*, 2002, **117**, 4709.

[90] T. A. Titarchuk and R. K. Halpern, *Chem. Phys. Lett.*, 1995, **232**, 192.

[91] J. C. Boden and B. A. Thrush, *Proc. R. Soc. London A*, 1968, **305**, 107.

[92] M. Y. Louge and R. K. Hanson, *Int. J. Chem. Kinet*, 1984, **16**, 231.

[93] D. F. Davidson, A. J. Dean, M. D. DiRosa, and R. K. Hanson, *Int. J. Chem. Kinet*, 1991, **23**, 1035.